Hindawi
Advances in High Energy Physics
Volume 2021, Article ID 9548737, 21 pages
https://doi.org/10.1155/2021/9548737

Research Article

Statistical Behavior of Lepton Pair Spectrum in the Drell-Yan Process and Signal from Quark-Gluon Plasma in High-Energy Collisions

Xu-Hong Zhang and Fu-Hu Liu

Institute of Theoretical Physics & Collaborative Innovation Center of Extreme Optics & State Key Laboratory of Quantum Optics and Quantum Optics Devices, Shanxi University, Taiyuan 030006, China

Correspondence should be addressed to Fu-Hu Liu; fuhuliu@163.com

Received 20 August 2020; Revised 29 March 2021; Accepted 11 May 2021; Published 1 June 2021

Academic Editor: Theocharis Kosmas

We analyze the transverse momentum (p_T) spectra of lepton pairs ($\ell\bar{\ell}$) generated in the Drell-Yan process, as detected in proton-nucleus (pion-nucleus) and proton-(anti)proton collisions by ten collaborations over a center-of-mass energy ($\sqrt{s_{NN}}$ or $\sqrt{s}$ if in a simplified form) range from ~ 20 GeV to above 10 TeV. Three types of probability density functions (the convolution of two Lévy-Tsallis functions, the two-component Erlang distribution, and the convolution of two Hagedorn functions) are utilized to fit and analyze the p_T spectra. The fit results are approximately in agreement with the collected experimental data. Consecutively, we obtained the variation law of related parameters as a function of $\sqrt{s}$ and invariant mass (Q). In the fit procedure, a given Lévy-Tsallis (or Hagedorn) function can be regarded as the probability density function of transverse momenta contributed by a single quark (q) or anti-quark ($\bar{q}$). The Drell-Yan process is then described by the statistical method.

1. Introduction

There are more than one processes that can generate a pair of charged leptons ($\ell\bar{\ell}$) in experiments of high-energy collisions. In 1970, Sidney Drell and Tung-Mow Yan firstly proposed $\ell\bar{\ell}$ production in a high-energy hadron scattering in a process we now call the "Drell-Yan" process [1]. In this process, a quark (q) in one hadron and an antiquark ($\bar{q}$) in another hadron are annihilated, and a virtual photon (γ^*) or Z boson is generated, which then decays into $\ell\bar{\ell}$. This process is expressed as $A + B \longrightarrow \gamma^*/Z + X \longrightarrow \ell + \bar{\ell} + X$, where A and B are collision hadrons and X denotes other particles produced in the collisions. The Drell-Yan process has been extensively studied experimentally, theoretically, and phenomenologically.

The literature about the theoretical description of the Drell-Yan process within quantum chromodynamics (QCD) is well known and settled [2–9]. The framework for the description of the transverse momentum dynamics [sometimes, indicated as Collins-Soper-Sterman (CSS) formalism] is summarized in the well-known book by John Collins [2]. Some recent reviews on the subject of transverse momentum distributions in the Drell-Yan process can be found in refs. [4–6] in which many works were cited. More theoretical works at both small and large p_T are available in literature [7–9]. At the same time, lots of phenomenological works were published in the past [10–15], recent [16–21], and very recent years [22–25].

Several phenomenological interpretations of experimental Drell-Yan data collected in the previous many years have been released by various groups, particularly in recent years where first extractions of quark transverse momentum distributions are becoming available from highly accurate theoretical descriptions of QCD perturbative ingredients. The factorization theorem for the Drell-Yan process allows to write the transverse momentum differential cross-section as a convolution of two transverse momentum-dependent (TMD) parton distribution functions (PDFs), which are, under certain conditions, very complicated. This complicated factorization involves soft

factors that resum soft gluon radiation regularizing a certain class of divergences that arise in the theoretical formulae. The soft gluon resummation is especially important in the description of the quark-gluon plasma (QGP), where $\ell\bar{\ell}$ can be produced in a process similar to that of Drell-Yan but with different origins of quarks.

QGP is a new form of matter which is created in the central region of high-energy nucleus-nucleus collisions, where extreme density and high-temperature environment are developed. It has become one of the important areas of research in the field of nuclear and particle physics. The gradual maturity of QCD and gauge field theory provides a powerful explanation for this novel matter and phenomenon. In fact, QGP is particularly short-lived. In QGP, a quark q and anti-quark $\bar{q}$ can soon be annihilated into a virtual photon γ^* or Z boson, which then decays to a pair of leptons $\ell\bar{\ell}$. This happens in the QGP degeneration process in which most particles are produced. The yield, invariant mass, rapidity (y), and transverse momentum (p_T) distribution of $\ell\bar{\ell}$ depend on the momentum distribution of $q\bar{q}$ and gluons in QGP in the collision region. Therefore, the information of $\ell\bar{\ell}$ can be used to judge whether QGP is generated and further to study its thermodynamic status making the $\ell\bar{\ell}$ production one of the most important signals generated by QGP. Consequently, the study on $\ell\bar{\ell}$ becomes particularly critical.

From the above, it is clear that $\ell\bar{\ell}$ can be produced in high-energy hadronic/nucleonic collisions in two main ways: the Drell-Yan process and QGP degeneration process. To study the properties of QGP, we should remove the influence of the Drell-Yan process and vice-versa. Generally, we may use the same methodology to describe the two processes. At present, one mainly uses the statistical method to study the properties of QGP. Correspondingly, we may also use the statistical method to study the production of $\ell\bar{\ell}$ in the Drell-Yan process, especially because the factorization theorem is very hard to model. In short, the statistical description for the Drell-Yan process is necessary to better understand the properties of QGP.

The measurement of lepton-pair physical quantities (including energy, p_T, and y) in experiments studying the Drell-Yan process provides lots of valuable information about the dynamic properties and evolution process of the produced particles. In particular, p_T is Lorentz invariant in the beam direction and can be used to describe the particles' motion and system's evolution. There are different functions that can be used to describe the $\ell\bar{\ell}p_T$ spectra in statistics. For example, we can use the Lévy-Tsallis function [26–30], the (two-component) Erlang distribution [31–33], and the Hagedorn function [34, 35] to fit the experimental data to obtain the analytical parameters of the p_T spectrum. Since the Drell-Yan process is the result of the interactions of q and $\bar{q}$, we can use the convolution of two functions to describe the p_T spectra. The idea of convolution is concordant to the factorization theorem for the Drell-Yan process.

In this paper, we use three functions to fit and analyze the Drell-Yan $\ell\bar{\ell}p_T$ spectra obtained by ten collaborations from the experiments of high-energy proton-nucleus (pion-nucleus) and proton-(anti)proton collisions. These experimental studies provide a great resource for us to better understand the collision mechanism and dynamic characteristics of the mentioned process.

2. Formalism and Method

Naturally, the p_T spectra of Drell-Yan $\ell\bar{\ell}$ depend on collision energy. For that reason, we should use different probability functions to study these spectra at different energies. Here, we briefly describe the three functions which will be used in this study. In the following, p_{t1} and p_{t2} are the transverse momenta of the two quarks, and p_T is the transverse momentum of the two quark system, which equals the transverse momentum of the dilepton system at leading order.

2.1. The Lévy-Tsallis Function. The Boltzmann distribution is the most important probability density function in thermodynamic and statistical physics. We present the probability density function of p_T as a simple Boltzmann distribution [36–38]:

$$f_{p_T}(p_T) = \frac{1}{N}\frac{dN}{dp_T} = C_B p_T \exp\left(-\frac{\sqrt{p_T^2 + m_0^2}}{T_B}\right), \quad (1)$$

where N is the number of identical particles of mass m_0 produced in the collisions, C_B is the normalization constant, and T_B is the effective temperature of the collision system.

The Boltzmann distribution is a special form of the Tsallis distribution, and the latter has a few alternative forms [26–30]. As one of the Tsallis distribution and its alternative forms, the Lévy-Tsallis function of the p_T spectrum of hadrons [26–30] is used in this work. We have the following form to describe the transverse momentum (p_t) distribution of (anti-)quark:

$$f_1(p_t) = N_q \sqrt{p_t}\left[1 + \frac{1}{nT}\left(\sqrt{p_t^2 + m_q^2} - m_q\right)\right]^{-n}, \quad (2)$$

where N_q is the normalization constant, T and n are the fitted parameters, and m_q is the mass of q or $\bar{q}$ taking part in the reaction. In general, we use $m_u = m_d = 0.3\text{GeV}/c^2$ in the Drell-Yan process because q or $\bar{q}$ is from the participant hadrons. The same m_u or m_d is for sea quarks and those in baryons, where the sea quarks of higher mass are not considered in this work. In QGP, $m_u = 0.003$ GeV/c^2 and $m_d = 0.007\text{GeV}/c^2$ because the quarks are approximately bare [39]. It has been verified that the Tsallis distribution is just a special case of the Lévy distribution, but not the opposite [30].

2.2. The (Two-Component) Erlang Distribution. The Erlang distribution [31–33] is proposed to fit the p_T spectra in the multisource thermal model [40]. Generally, a two-component Erlang distribution [31–33] is used to describe both the soft and hard processes. The contribution fractions of the two components are determined by fitting the experimental data. The numbers of parton sources participating in the soft and hard processes are represented by $n_S \geq 2$ and $n_H = 2$, respectively. The contribution

(p_t) of each parton source to p_T of final-state particle is assumed to obey an exponential function:

$$f_i(p_t) = \frac{1}{\langle p_t \rangle} \exp\left(-\frac{p_t}{\langle p_t \rangle}\right), \quad (3)$$

where $\langle p_t \rangle$ represents the average p_t contributed by the i-th source. Because $\langle p_t \rangle$ is the same for different sources, the index i in $\langle p_t \rangle_i$ is omitted.

The p_T distribution contributed by n_S (n_H) sources is the convolution of n_S (n_H) exponential functions, which gives the Erlang distribution. Let k denote the contribution fraction of the first component (soft process). The two-component Erlang distribution is

$$f(p_T) = \frac{k p_T^{n_S-1}}{(n_S-1)!\langle p_t \rangle_S^{n_S}} \exp\left(-\frac{p_T}{\langle p_t \rangle_S}\right) + \frac{(1-k)p_T}{\langle p_t \rangle_H^2} \exp\left(-\frac{p_T}{\langle p_t \rangle_H}\right). \quad (4)$$

Fitting the data with the two-component Erlang distribution, we can get the changes of parameters $\langle p_t \rangle_S$, $\langle p_t \rangle_H$, and k.

We should discuss the values of n_S and n_H further. If $n_S > 2$, the participant partons are expected to be $q\bar{q}$ and $n_S - 2$ gluons in the soft or nonviolent annihilation process. Considering that the probability of multiparton participating together in the process is low, we have usually $n_S = 2$ or 3 in this work. Generally, the larger the n_S, the sharper the distribution peak. In many cases, $n_S = 3$ means that $q\bar{q}$ and a gluon participate in the soft process. For all cases, $n_H = 2$ (always true in this work) means that only $q\bar{q}$ participates in the violent annihilation in the hard process.

2.3. The Hagedorn Function. The Hagedorn function is an inverse power law [34, 35] which is an empirical formula derived from perturbative QCD. Generally, this function can only describe the spectra at large p_T, but not the entire p_T interval. In the case of using the Hagedorn function in a wide range of p_T, the probability density function of p_T can be expressed as

$$f_1(p_T) = A p_T \left(1 + \frac{p_T}{p_1}\right)^{-n_1}, \quad (5)$$

where A is the normalization constant, and p_1 and n_1 are the fitted parameters. The final-state particles with high momenta are mainly produced by the hard scattering process during the collisions. However, both the soft and hard processes contribute to the p_T spectra. In some cases, the soft excitation process in the low p_T range can also be described by the Hagedorn function. We try to use the Hagedorn function to describe the transverse momentum distribution of (anti-)quarks. That is, we may use p_t instead of p_T in Eq. (5) to obtain the transverse momentum distribution of (anti-)quarks, which is a new form of Eq. (5) and will be used in the following section.

We have tested the Hagedorn function with different revisions in which p_T/p_1 in Eq. (5) is replaced by p_T^2/p_1^2, $A p_T$ is replaced by $A p_T^2/m_T$, or p_T/p_1 is replaced by p_T^2/p_1^2, and $A p_T$ is replaced by A, where p_1 and A vary in different revisions. The uses of the revised Hagedorn functions result in some overestimations in low (or high) p_T region comparing to the Hagedorn function. Contrarily, these revisions result in some underestimations in high (or low) p_T region due to the normalization. The revisions of the Hagedorn function are beyond the focus of the present work, and we shall not discuss them further.

2.4. The Convolution of Functions. The convolution of functions is an important operation process in functional analysis that can be used to describe the weighted superposition of input and system response (that is, two subfunctions). The Drell-Yan process is the result of the interactions of q and $\bar{q}$ in high-energy collisions, which means that we need the convolution of two functions to describe this process. Indeed, the above Eq. (2) or (5) can be used to describe the transverse momentum distribution, $f_1(p_{t1})$, of a single (anti-)quark's contribution. The second (anti-)quark's contribution is $f_2(p_{t2}) = f_1(p_T - p_{t1})$, where p_T is still the transverse momentum of the $\ell\bar{\ell}$ system. So, the convolution of two probability density functions should be used to describe the p_T spectrum of $\ell\bar{\ell}$ in the Drell-Yan process. We have the convolution of two Eq. (2) or (5) to be expressed as

$$f(p_T) = \int_0^{p_T} f_1(p_{t1}) f_1(p_T - p_{t1}) dp_{t1}, \quad (6)$$

where $f_1(p_{t1})$ [$f_1(p_T - p_{t1})$] is shown as Eq. (2) if we use the Lévy-Tsallis function or Eq. (5) if we use the Hagedorn function.

It should be noted that the total transverse momentum before (of the two quarks system) and after (of the two leptons system) are equal. The assumption that the total transverse momentum is equal to the sum of the scalar transverse momenta of the two partons that is for the particular case in which the vectors $\vec{p}_{t1}$ and $\vec{p}_{t2}$ are parallel. Our recent works [41, 42] show that this assumption is in agreement with many data. Naturally, we do not rule out other assumptions such as the particular case in which $\vec{p}_{t1}$ and $\vec{p}_{t2}$ are perpendicular and the general case which shows any azimuth for $\vec{p}_{t1}$ and $\vec{p}_{t2}$. The particular case used in this work is more easier than other particular or general case in the fit to data. We are inclined to use the parallel case.

As a legitimate treatment, the convolution formula Eq. (6) can be used to fit the p_T spectrum of $\ell\bar{\ell}$ in the Drell-Yan process, where $f_1(p_{t1})$ and $f_1(p_T - p_{t1})$ are from empirical guess which is simpler than the factorization theorem based on perturbative QCD. On one hand, Eq. (6) can reflect the weighted contribution of the transverse momentum of each (anti-)quark to the p_T spectrum in the process. On the other hand, Eq. (6) can also reflect the system in which two main participants take part in the interactions. Using the convolution to fit the data is a good choice for us, which allows us to

more accurately understand the interaction process and mechanism between interacting partons, more completely describe the energy dependence and interdependence of the function parameters, and further better analyze the p_T spectrum.

3. Results and Discussion

3.1. Comparison with Data. Figure 1 shows the p_T spectra of $\ell\bar{\ell}$ [with different invariant masses (Q) or Feynman variables (x_F)] produced by the Drell-Yan process in different collisions at different energies (with different integral luminosities if available in literature), where the concrete type of $\ell\bar{\ell}$ is also given in each panel. The symbols E and σ on the vertical axis denote the energy of $\ell\bar{\ell}$ and the cross-section of events, respectively. Among them, the data points presented in Figures 1(a)–1(c) are quoted from the proton-copper (p-Cu) collision experiments performed by the E288 Collaboration [43], and the collision energy per nucleon pair ($\sqrt{s_{NN}}$ or $\sqrt{s}$ if in a simplified form) is 19.4, 23.8, and 27.4 GeV, respectively. The data points shown in Figure 1(d) are the results of the p-Cu collision experiment performed by the E605 Collaboration [44] at a collision energy of 38.8 GeV. For the E288 Collaboration, the invariant mass ranges from 4 to 14GeV/c^2, while the corresponding invariant mass ranges of the E605 Collaboration are from 7 to 18GeV/c^2. The experimental data points in Figures 1(e) and 1(f) are from negative pions (π^-) induced wolfram (W) (π^--W) collisions at 21.7 GeV performed by the FNAL-615 Collaboration [45]. The different symbols in Figure 1(e) represent invariant mass Q in the range of 4.05–13.05GeV/c^2 with different scalings, where the units GeV/c^2 are not shown in the panel due to crowding space. The Feynman variables range from 0 to 1 with a step of 0.1, as shown in Figure 1(f). Different collaborations have different intervals of Q and x_F, while the detailed binning information is marked in the panels. In some cases, the range of rapidity y is not available due to other selection conditions such as the complex polar coverages and sensitivities of detector components or Feynman variable being used [45]. The total experimental uncertainties are cited from refs. [43–45] which include both the statistical and systematic uncertainties if both are available. The solid, dashed, and dotted curves in all panels are the results of our fittings with the convolution of two Lévy-Tsallis functions, the two-component Erlang distribution, and the convolution of two Hagedorn functions, respectively. The histograms in this and following figure correspond to QCD calculations which will be discussed later. We use the minimum-χ^2 to evaluate the goodness of the fits, where $\chi^2 = \sum_j[(\text{Data}_j - \text{Fit}_j)^2/\text{Uncertainty}_j^2]$ and j are for the j-th data. We list the results of the fits (parameters), the χ^2 and the number of degrees of freedom (ndof) in Table 1. The numbers $n_S = 3$ and $n_H = 2$ which are not listed in the table to avoid trivialness. One can see that the three functions can approximately describe the p_T spectra of $\ell\bar{\ell}$ produced by the Drell-Yan process in high-energy p-Cu and π^--W collisions. The two-component Erlang distribution describes better than the other two functions.

Figure 2 shows the p_T spectra of $\ell\bar{\ell}$ (with different invariant mass Q) generated by the Drell-Yan process in proton-proton (p-p or pp) collisions and measured by three different collaborations. The data points in Figure 2(a) are from the experimental results measured by the R209 Collaboration [46]. The collision energy is $\sqrt{s} = 62$GeV, and the Q range is $5 - 8\text{GeV}/c^2$. The data points in Figure 2(b) show the experimental results from the PHENIX Collaboration [47]. The $\sqrt{s}$ is 200 GeV, the Q range is $4.8 - 8.2\text{GeV}/c^2$, and the rapidity range is $1.2 < y < 2.2$. The data points in Figure 2(c) are from the experimental results of the STAR Collaboration [24]. The $\sqrt{s}$ is 510 GeV, the Q range is 73 – 114GeV/c^2, and the rapidity range is $|y| < 1$. In some cases, the range of rapidity y is not available due to other selection conditions being used [46]. The curves of the three fits are also shown. and the extracted parameters are presented in Table 2. One can see that the three functions can approximately describe the p_T spectra of $\ell\bar{\ell}$ produced by the Drell-Yan process in high-energy pp collisions.

Similar to Figure 2, Figure 3 shows the p_T spectra of $\ell\bar{\ell}$ produced by the Drell-Yan process in proton-antiproton (p-$\bar{p}$ or $p\bar{p}$) collisions with $66 \le Q < 116$ GeV/c^2(Figures 3(a) and 3(b)),$75 \le Q < 105\text{GeV}/c^2$ (Figure 3(c)), and $70 \le Q < 110\text{GeV}/c^2$ (Figure 3(d)) at$\sqrt{s} = 1.8$TeV (Figures 3(a) and 3(c)) and $\sqrt{s} = 1.96$TeV (Figures 3(b) and 3(d)). The data points in Figures 3(a) and 3(b) are from the experiments of the CDF [48, 49] and D0 Collaborations [50–52], respectively. In some cases, the range of rapidity y is not available due to other selection conditions being used [48–50]. The curves of the three fits are also shown, and the extracted parameters are presented in Table 2. One can see that the three functions can approximately describe the p_T spectra of $\ell\bar{\ell}$ produced by the Drell-Yan process in high-energy $p\bar{p}$ collisions.

Figure 4 shows the p_T spectra of $\ell\bar{\ell}$ produced by the Drell-Yan process in high-energy pp collisions, where the data used in the figure are all examples and there is no bias towards any specific CERN experiment. From Figures 4(a)–4(f), the event samples [with different conditions ($\sqrt{s}$, Q, and y)] are shown in the panels. The data points are quoted from the experiments performed by the ATLAS (Figures 4(a)–4(d)) [53–55], CMS (Figure 4(e)) [56, 57], and LHCb Collaborations (Figure 4(f)) [58–60]. The extracted fit parameter values are listed in Table 2. One can see that the three functions can approximately describe the p_T spectra of $\ell\bar{\ell}$ produced by the Drell-Yan process in pp collisions at ultrahigh energies.

From the above comparisons, we see that some of the data sets are relatively poorly described by the fit. Notably, the FNAL-615 data, and the CDF data at 1.96 TeV, are not very well fitted. Specifically, the fit of the CDF data returns a poor χ^2, unlike the other Tevatron experiments, as all LHC data sets have reasonably good χ^2. We would like to point out that the relatively poor χ^2 of some data is understandable due to the fact that the fit function works well in most cases and does not work well in a few cases. In addition, the data at high transverse momentum has low statistics which causes large dispersion of the data from the fit. In other cases, the low statistics happen to be well fitted. To improve

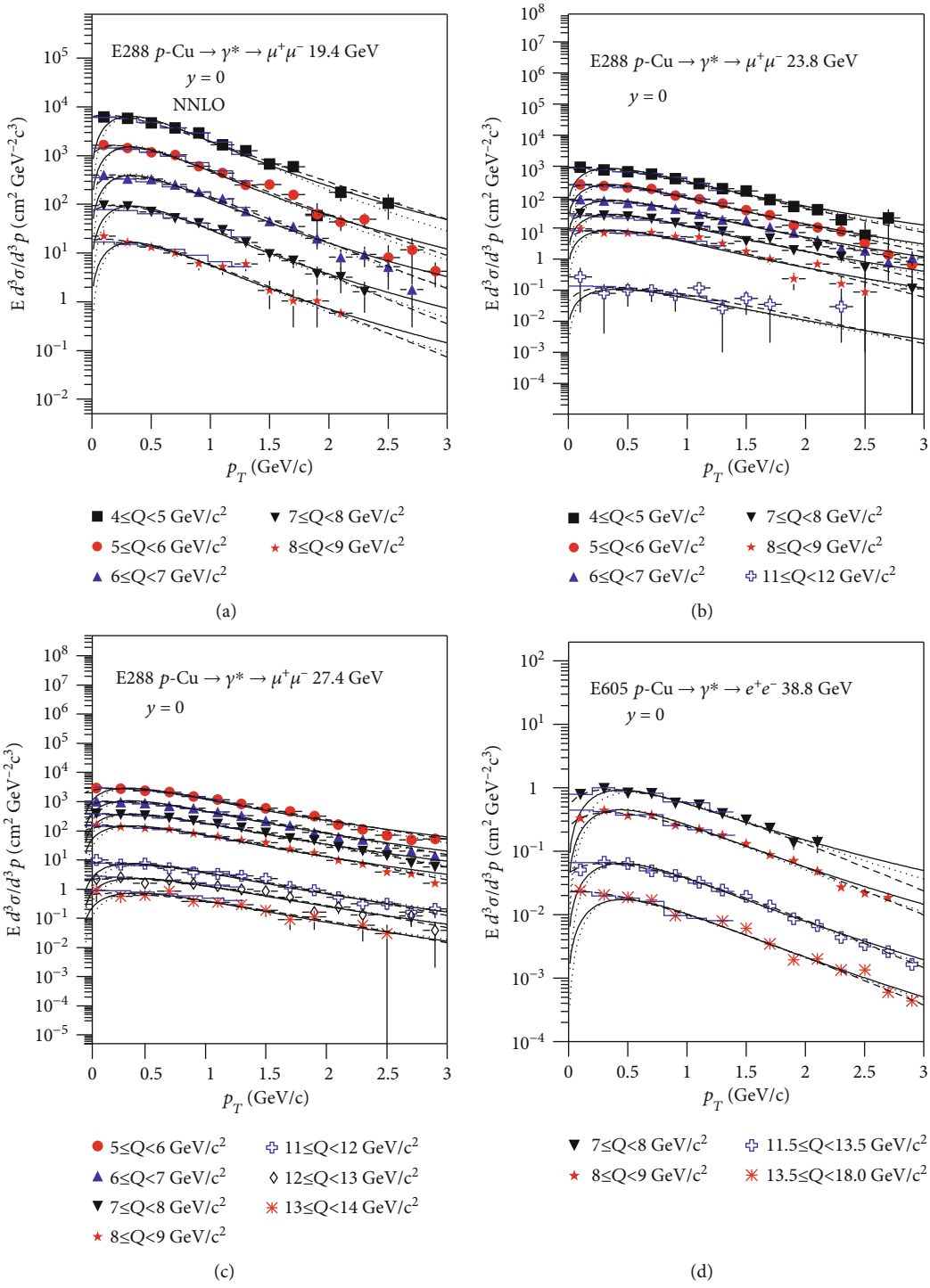

Figure 1: Continued.

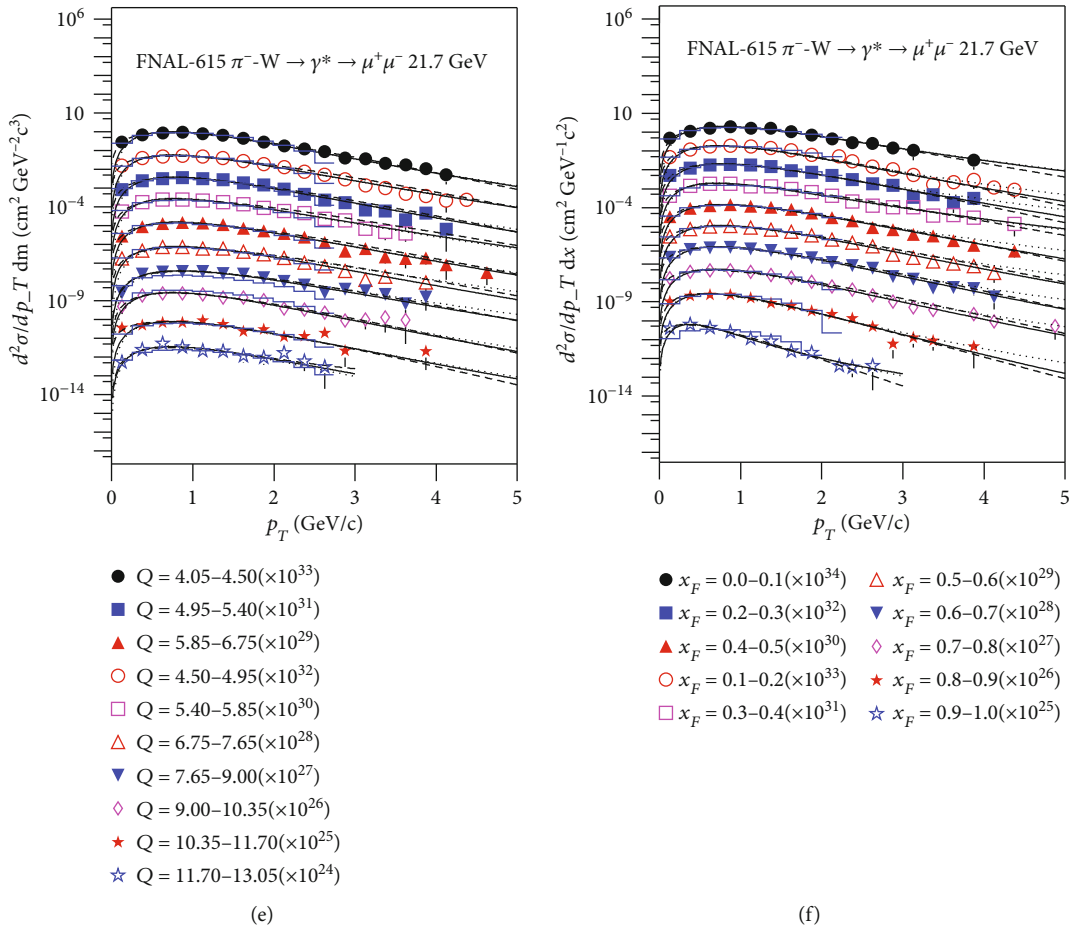

FIGURE 1: Transverse momentum spectra of $\ell\bar{\ell}$ (with different invariant masses Q or Feynman variables x_F) produced by the Drell-Yan process in different collisions at different energies. The data points in (a)–(c) are quoted from the E288 Collaboration [43] and obtained in p-Cu collisions at $\sqrt{s} = 19.4$ GeV ($4 \le Q < 9 GeV/c^2$), 23.8 GeV ($4 \le Q < 13 GeV/c^2$), and 27.4 GeV ($5 \le Q < 13 GeV/c^2$), respectively. The data points in (d) come from p-Cu collisions at $\sqrt{s} = 38.8$ GeV performed by the E605 Collaboration [44]. The data points in (e) ($4.05 \le Q < 13.05 GeV/c^2$) and (f) ($0.0 \le x_F < 1.0$) come from π^--W collisions at $\sqrt{s} = 21.7$ GeV measured by the FNAL-615 Collaboration [45], where the units GeV/c^2 are not shown in (e) due to crowding space. In panel (d), $\ell\bar{\ell}$ is e^+e^-, and in other panels, $\ell\bar{\ell}$ is $\mu^+\mu^-$. The solid, dashed, and dotted curves are our results of fitting the data points with the convolution of two Lévy-Tsallis functions [Eqs. (2) and (6)], the two-component Erlang distribution [Eq. (4)], and the convolution of two Hagedorn functions [Eqs. (5) and (6)], respectively, see text in subsection 3.3 for the meanings of histograms which are quoted from QCD calculations.

the relatively poor χ^2 of some fits, a better fit function could be used in the future; although, it is not feasible to find a fit function that works well in all cases. One could improve the quality of the fits by concentrating in the high-statistic regions or by rebinning the low-statistic data.

3.2. Tendency of Parameters. In order to study the underlying law that governs the variation of the extracted parameters with $\sqrt{s}$ and Q, we preset the values of the fitted parameters as a function of the these two quantities. Figures 5(a) and 5(b) show the trend of parameter n, and Figures 5(c) and 5(d) show the trend of parameter T, obtained by the fitting, using the Lévy-Tsallis function. Comparing Figures 5(a) and 5(c), we can analyze the dependence of parameters on $\sqrt{s}$. On average, it can be seen that as $\sqrt{s}$ increases, the parameter n increases quickly and then decreases slowly, and the parameter T increases slowly and then significantly. There is a knee point for the trend of n at $\sqrt{s} \approx 40$–50 GeV. Meanwhile, there is a boundary at $\sqrt{s} \approx 200$–500 GeV above which T increases significantly. Similarly, we compare Figures 5(b) and 5(d) and analyze the variation of parameters with Q. It can be clearly seen that the parameter n increases firstly and then decreases, and the parameter T increases slowly and then significantly, with the increase of Q. There is a knee point for the trend of n at $Q \approx 14$–15 GeV/c^2. Meanwhile, there is a boundary at $Q \approx 20$–60 GeV/c^2 above which T increases significantly.

Figure 6 is similar to Figure 5, but shows the dependence of parameters $\langle p_t \rangle_S$ (Figures 6(a) and 6(b)), $\langle p_t \rangle_H$ (Figures 6(c) and 6(d)), and k (Figures 6(e) and 6(f)) on $\sqrt{s}$(Figures 6(a), 6(c), and 6(e)) andQ (Figures 6(b), 6(d), and 6(f)) obtained from the two-component Erlang distribution. One can see that with increasing $\sqrt{s}$, $\langle p_t \rangle_S$ and $\langle p_t \rangle_H$ increase slowly and then

Table 1: Values of parameters n and T in the Lévy-Tsallis function (solid curves), $\langle p_t \rangle_S$, $\langle p_t \rangle_H$, and k in the two-component Erlang distribution (dashed curves), as well as p_1 and n_1 in the Hagedorn function (dotted curves) in Figure 1. The χ^2 is for each fit. The ndof is for the fits of the two-component Erlang distribution. For the fits of Lévy-Tsallis function and Hagedorn function, the ndof needs one more. For Figure 1(f), the selection is not the invariant mass Q, but the Feynman variable x_F. $n_S = 3$ and $n_H = 2$ for Figure 1, which are not listed in the table.

Figure	$\sqrt{s}$ (GeV)	Q (GeV/c^2)	n	T (GeV)	χ^2	$\langle p_t \rangle_S$ (GeV/c)	$\langle p_t \rangle_H$ (GeV/c)	k	χ^2	p_1 (GeV/c)	n_1	χ^2	ndof
Figure 1(a)	19.4	4-5	3.910 ± 0.089	0.161 ± 0.005	122	0.294 ± 0.003	0.611 ± 0.006	0.961 ± 0.003	52	1.028 ± 0.006	6.994 ± 0.022	164	10
		5-6	3.969 ± 0.089	0.166 ± 0.005	82	0.303 ± 0.004	0.608 ± 0.006	0.974 ± 0.003	24	1.031 ± 0.006	6.992 ± 0.022	99	11
		6-7	4.008 ± 0.090	0.169 ± 0.005	34	0.327 ± 0.006	0.588 ± 0.005	0.978 ± 0.003	10	1.035 ± 0.006	6.987 ± 0.022	43	10
		7-8	4.139 ± 0.093	0.171 ± 0.005	9	0.331 ± 0.008	0.511 ± 0.004	0.973 ± 0.003	1	1.046 ± 0.006	6.944 ± 0.021	12	8
		8-9	4.155 ± 0.098	0.176 ± 0.005	6	0.348 ± 0.008	0.494 ± 0.004	0.961 ± 0.003	3	1.049 ± 0.006	6.921 ± 0.020	8	7
Figure 1(b)	23.8	4-5	3.571 ± 0.087	0.181 ± 0.006	155	0.318 ± 0.004	0.642 ± 0.006	0.964 ± 0.003	13	1.002 ± 0.005	6.264 ± 0.016	157	11
		5-6	3.892 ± 0.089	0.182 ± 0.006	96	0.339 ± 0.005	0.598 ± 0.005	0.967 ± 0.003	22	1.003 ± 0.004	6.264 ± 0.015	99	11
		6-7	3.909 ± 0.092	0.195 ± 0.007	67	0.364 ± 0.007	0.579 ± 0.005	0.961 ± 0.003	15	1.005 ± 0.004	6.230 ± 0.015	74	11
		7-8	3.988 ± 0.089	0.196 ± 0.007	38	0.379 ± 0.008	0.543 ± 0.005	0.970 ± 0.003	14	1.010 ± 0.004	6.194 ± 0.013	40	10
		8-9	4.135 ± 0.102	0.197 ± 0.007	42	0.380 ± 0.008	0.494 ± 0.004	0.974 ± 0.003	31	1.011 ± 0.004	6.193 ± 0.014	42	9
		11-12	4.410 ± 0.114	0.241 ± 0.010	3	0.427 ± 0.011	0.433 ± 0.004	0.982 ± 0.003	3	1.025 ± 0.005	6.021 ± 0.012	4	6
Figure 1(c)	27.4	5-6	3.264 ± 0.060	0.187 ± 0.006	103	0.367 ± 0.006	0.773 ± 0.007	0.947 ± 0.003	35	1.030 ± 0.005	6.164 ± 0.010	159	11
		6-7	3.760 ± 0.084	0.202 ± 0.008	184	0.386 ± 0.008	0.711 ± 0.006	0.953 ± 0.003	88	1.041 ± 0.005	6.144 ± 0.009	180	11
		7-8	3.653 ± 0.088	0.213 ± 0.009	144	0.403 ± 0.008	0.688 ± 0.006	0.953 ± 0.003	38	1.067 ± 0.005	6.136 ± 0.010	165	11
		8-9	3.905 ± 0.092	0.217 ± 0.009	109	0.409 ± 0.008	0.638 ± 0.006	0.953 ± 0.003	45	1.082 ± 0.006	6.125 ± 0.010	122	11
		11-12	4.247 ± 0.106	0.230 ± 0.012	21	0.442 ± 0.010	0.602 ± 0.005	0.931 ± 0.003	10	1.081 ± 0.005	6.093 ± 0.009	27	11
		12-13	4.466 ± 0.113	0.253 ± 0.014	15	0.464 ± 0.011	0.564 ± 0.005	0.944 ± 0.003	11	1.086 ± 0.006	6.089 ± 0.009	16	10
		3-14	4.986 ± 0.133	0.256 ± 0.014	4	0.468 ± 0.011	0.552 ± 0.005	0.944 ± 0.003	3	1.084 ± 0.006	6.092 ± 0.009	4	8
Figure 1(d)	38.8	7-8	3.211 ± 0.064	0.254 ± 0.013	19	0.446 ± 0.010	0.654 ± 0.006	0.983 ± 0.003	6	1.257 ± 0.009	6.191 ± 0.010	42	7
		8-9	4.371 ± 0.080	0.262 ± 0.013	47	0.469 ± 0.012	0.602 ± 0.006	0.992 ± 0.003	11	1.180 ± 0.008	6.201 ± 0.011	52	10
		11.5-13.5	4.694 ± 0.118	0.267 ± 0.013	32	0.473 ± 0.013	0.529 ± 0.005	0.995 ± 0.003	7	1.194 ± 0.007	6.190 ± 0.010	44	11
		13.5-18.0	4.949 ± 0.131	0.278 ± 0.015	94	0.480 ± 0.013	0.434 ± 0.007	0.986 ± 0.003	34	1.197 ± 0.007	6.171 ± 0.012	98	10
Figure 1(e)	21.7	4.05-4.50	3.221 ± 0.085	0.155 ± 0.005	412	0.397 ± 0.008	0.473 ± 0.013	0.958 ± 0.003	107	0.572 ± 0.006	2.175 ± 0.012	563	13
		4.50-4.95	3.073 ± 0.073	0.163 ± 0.005	227	0.429 ± 0.009	0.314 ± 0.005	0.968 ± 0.003	94	0.505 ± 0.005	2.696 ± 0.010	311	14
		4.95-5.40	3.663 ± 0.089	0.176 ± 0.006	122	0.411 ± 0.008	0.481 ± 0.014	0.966 ± 0.003	88	0.512 ± 0.005	2.357 ± 0.014	180	13
		5.40-5.85	3.348 ± 0.088	0.165 ± 0.005	47	0.425 ± 0.009	0.632 ± 0.016	0.955 ± 0.003	57	0.595 ± 0.005	2.803 ± 0.012	79	11
		5.85-6.75	3.841 ± 0.112	0.186 ± 0.008	44	0.428 ± 0.009	0.358 ± 0.006	0.977 ± 0.003	55	0.551 ± 0.005	2.540 ± 0.014	68	14
		6.75-7.65	3.453 ± 0.088	0.188 ± 0.008	32	0.442 ± 0.010	0.499 ± 0.015	0.971 ± 0.003	48	0.563 ± 0.005	2.746 ± 0.015	70	11
		7.65-9.00	3.965 ± 0.090	0.202 ± 0.008	20	0.433 ± 0.010	0.423 ± 0.009	0.997 ± 0.003	28	0.552 ± 0.005	2.323 ± 0.014	33	12

Table 1: Continued.

Figure	$\sqrt{s}$ (GeV)	Q (GeV/c^2)	n	T (GeV)	χ^2	$\langle p_t \rangle_S$ (GeV/c)	$\langle p_t \rangle_H$ (GeV/c)	k	χ^2	p_1 (GeV/c)	n_1	χ^2	ndof
		9.00-10.35	3.321 ± 0.088	0.167 ± 0.005	15	0.379 ± 0.007	0.482 ± 0.014	0.983 ± 0.003	10	0.506 ± 0.005	2.904 ± 0.018	20	11
		10.35-11.70	3.013 ± 0.073	0.172 ± 0.005	17	0.372 ± 0.007	0.219 ± 0.003	0.984 ± 0.003	13	0.561 ± 0.005	2.767 ± 0.016	20	9
		11.70-13.05	2.707 ± 0.045	0.153 ± 0.005	3	0.354 ± 0.006	1.491 ± 0.057	0.979 ± 0.003	3	0.521 ± 0.005	3.312 ± 0.025	3	7
		x_F (1/c)											
		0.00-0.10	2.702 ± 0.045	0.148 ± 0.005	32	0.408 ± 0.008	0.645 ± 0.016	0.974 ± 0.003	15	0.189 ± 0.005	2.035 ± 0.008	47	11
		0.10-0.20	2.873 ± 0.048	0.113 ± 0.004	69	0.374 ± 0.007	0.503 ± 0.015	0.976 ± 0.003	25	0.188 ± 0.005	2.806 ± 0.012	92	15
		0.20-0.30	3.978 ± 0.092	0.187 ± 0.006	90	0.386 ± 0.008	0.487 ± 0.014	0.979 ± 0.003	46	0.190 ± 0.005	2.865 ± 0.012	134	13
		0.30-0.40	2.938 ± 0.058	0.136 ± 0.005	120	0.393 ± 0.008	0.580 ± 0.015	0.963 ± 0.003	62	0.184 ± 0.005	2.468 ± 0.011	159	13
Figure 1(f)	21.7	0.40-0.50	3.046 ± 0.061	0.152 ± 0.005	105	0.393 ± 0.008	0.512 ± 0.014	0.975 ± 0.003	57	0.185 ± 0.005	3.581 ± 0.018	190	13
		0.50-0.60	2.820 ± 0.052	0.158 ± 0.005	106	0.399 ± 0.008	0.491 ± 0.014	0.959 ± 0.003	54	0.293 ± 0.010	3.302 ± 0.016	162	13
		0.60-0.70	2.721 ± 0.045	0.180 ± 0.006	141	0.383 ± 0.008	0.403 ± 0.012	0.969 ± 0.003	52	0.298 ± 0.010	2.841 ± 0.012	198	13
		0.70-0.80	2.938 ± 0.048	0.158 ± 0.005	119	0.376 ± 0.007	0.427 ± 0.013	0.956 ± 0.003	55	0.202 ± 0.008	3.102 ± 0.016	166	13
		0.80-0.90	3.022 ± 0.063	0.126 ± 0.004	74	0.284 ± 0.004	0.394 ± 0.011	0.989 ± 0.003	46	0.367 ± 0.012	3.673 ± 0.018	101	11
		0.90-1.00	3.143 ± 0.068	0.095 ± 0.012	25	0.195 ± 0.002	0.281 ± 0.008	0.985 ± 0.003	6	0.386 ± 0.015	3.868 ± 0.022	17	7

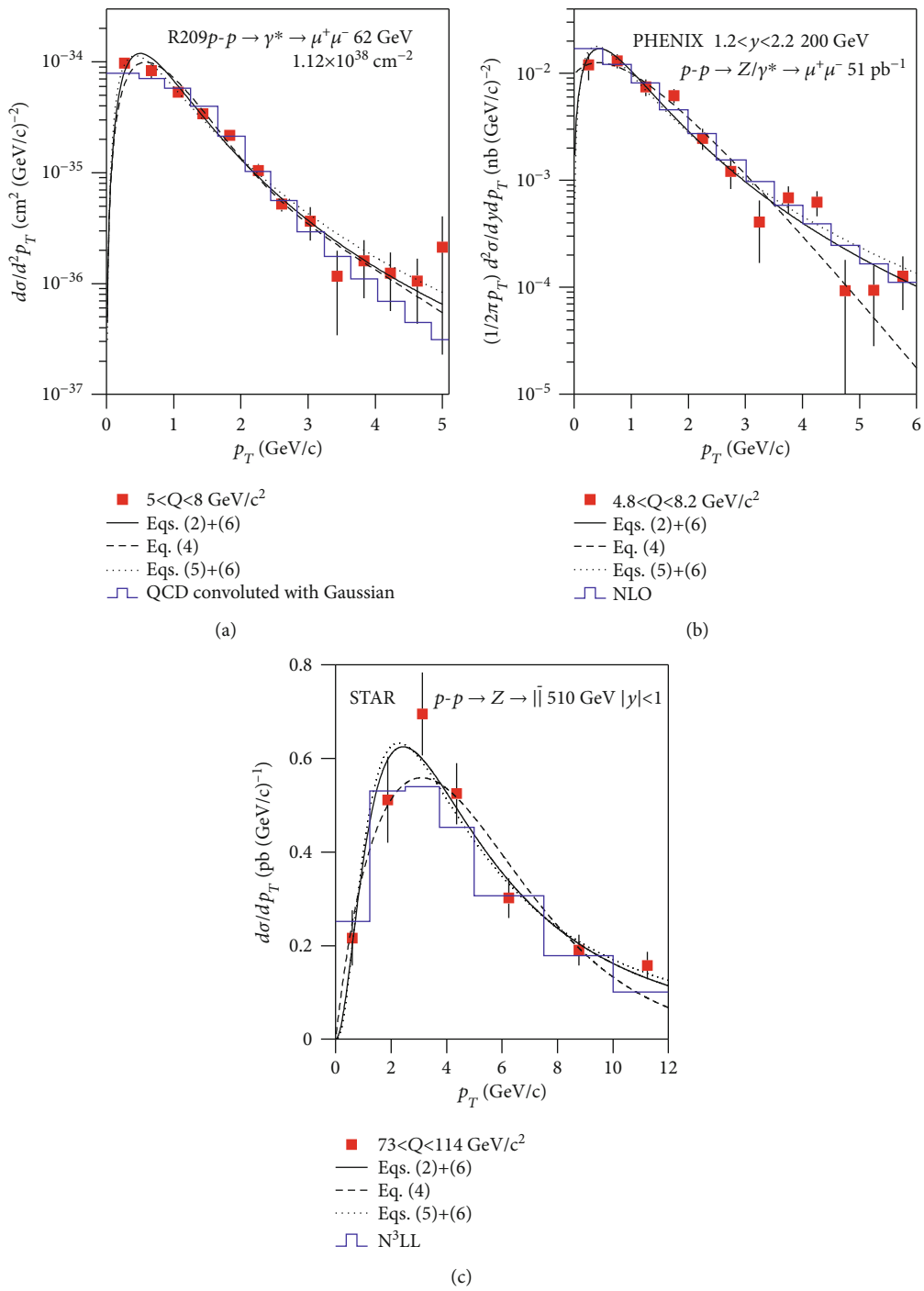

Figure 2: Transverse momentum spectra of $\ell\bar{\ell}$ (with different invariant masses Q) produced by the Drell-Yan process in pp collisions at $\sqrt{s} = 62$ (a), 200 (b), and 510 GeV (c). The data points are quoted from the R209 (a) [46], PHENIX (b) [47], and STAR Collaborations (c) [24]. In panels (a) and (b), $\ell\bar{\ell}$ is $\mu^+\mu^-$. The solid, dashed, and dotted curves are our results of fitting the data points with the convolution of two Lévy-Tsallis functions [Eqs. (2) and (6)], the two-component Erlang distribution [Eq. (4)], and the convolution of two Hagedorn functions [Eqs. (5) and (6)], respectively, see text in subsection 3.3 for the meanings of histograms which are quoted from QCD calculations.

quickly, and k decreases slowly and then quickly. For $\sqrt{s}$, there is a boundary between 60 and 500 GeV for $\langle p_t \rangle_S$, between 500 and 1100 GeV for $\langle p_t \rangle_H$, and between 200 and 500 GeV for k. Meanwhile, with increasing Q, $\langle p_t \rangle_S$ and $\langle p_t \rangle_H$ increase slowly and then quickly, and k decreases slowly and then quickly. There is a boundary at $Q \approx 20$–60 GeV/c^2.

In Figure 7, we show the parameters from the fits using the Hagedorn function and their dependence on collision energy

Table 2: Values of parameters n and T in the Lévy-Tsallis function (solid curves), $\langle p_t \rangle_S$, $\langle p_t \rangle_H$, and k in the two-component Erlang distribution (dashed curves), as well as p_1 and n_1 in the Hagedorn function (dotted curves) in Figures 2–4. The χ^2 is for each fit. The ndof is for the fits of the two-component Erlang distribution. For the fits of the Lévy-Tsallis function and Hagedorn function, the ndof needs one more. For Figures 4(a) and 4(b), different y ranges are included. $n_S = 3$ and $n_H = 2$ for Figures 2 and 4, as well as $n_S = 2$ and $n_H = 2$ for Figure 3, which are not listed in the table.

Figure	$\sqrt{s}$ (GeV)	Q (GeV/c^2)	n	T (GeV)	χ^2	$\langle p_t \rangle_S$ (GeV/c)	$\langle p_t \rangle_H$ (GeV/c)	k	χ^2	p_1 (GeV/c)	n_1	χ^2	ndof
Figure 2(a)	62.0	5-8	3.887 ± 0.080	0.136 ± 0.006	21	0.287 ± 0.006	0.913 ± 0.075	0.989 ± 0.003	26	1.001 ± 0.005	6.829 ± 0.018	18	9
Figure 2(b)	200	4.8-8.2	3.187 ± 0.068	0.258 ± 0.015	18	0.617 ± 0.017	0.277 ± 0.010	0.977 ± 0.003	18	1.111 ± 0.005	5.089 ± 0.016	15	8
Figure 2(c)	510	73-114	3.162 ± 0.065	0.792 ± 0.018	4	1.924 ± 0.062	1.103 ± 0.110	0.801 ± 0.003	11	1.077 ± 0.012	3.137 ± 0.019	4	3
Figure 3(a)	1800	66-116	2.618 ± 0.028	0.820 ± 0.016	25	2.631 ± 0.110	7.092 ± 0.320	0.511 ± 0.002	24	1.088 ± 0.012	2.916 ± 0.015	37	33
Figure 3(b)	1960	66-116	2.661 ± 0.018	0.840 ± 0.018	270	2.690 ± 0.128	8.120 ± 0.403	0.524 ± 0.002	134	1.222 ± 0.013	3.030 ± 0.016	476	53
Figure 3(c)	1800	75-105	2.588 ± 0.021	0.779 ± 0.016	16	2.721 ± 0.101	8.151 ± 0.400	0.539 ± 0.002	16	1.040 ± 0.012	2.934 ± 0.015	30	14
Figure 3(d)	1960	70-110	2.745 ± 0.017	0.904 ± 0.017	14	2.830 ± 0.110	8.580 ± 0.450	0.539 ± 0.002	13	1.359 ± 0.015	3.106 ± 0.017	26	9
Figure 4(a)	7000	66-116											
		$0 \le \lvert y \rvert < 1$	2.415 ± 0.016	0.996 ± 0.016	3	3.521 ± 0.201	10.710 ± 0.501	0.450 ± 0.002	3	1.241 ± 0.013	2.780 ± 0.015	11	10
		$1 \le \lvert y \rvert < 2$	2.396 ± 0.016	1.003 ± 0.016	2	3.520 ± 0.201	10.793 ± 0.501	0.439 ± 0.002	3	1.231 ± 0.012	2.760 ± 0.015	7	10
		$2 \le \lvert y \rvert < 2.4$	2.336 ± 0.012	0.980 ± 0.016	1	3.482 ± 0.200	11.742 ± 0.507	0.434 ± 0.002	1	1.121 ± 0.012	2.679 ± 0.014	1	10
Figure 4(b)	8000	66-116											
		$0.0 \le \lvert y \rvert < 0.4$	2.385 ± 0.023	1.023 ± 0.018	2	3.520 ± 0.201	10.571 ± 0.505	0.425 ± 0.002	2	1.232 ± 0.012	2.738 ± 0.015	6	7
		$0.4 \le \lvert y \rvert < 0.8$	2.405 ± 0.023	1.031 ± 0.020	2	3.549 ± 0.203	10.713 ± 0.509	0.432 ± 0.002	2	1.266 ± 0.013	2.761 ± 0.016	6	7
		$0.8 \le \lvert y \rvert < 1.2$	2.411 ± 0.031	1.031 ± 0.019	2	3.561 ± 0.210	11.760 ± 0.515	0.438 ± 0.002	2	1.267 ± 0.013	2.767 ± 0.016	6	7
		$1.2 \le \lvert y \rvert < 1.6$	2.384 ± 0.023	1.031 ± 0.020	2	3.663 ± 0.213	11.106 ± 0.524	0.438 ± 0.002	1	1.267 ± 0.013	2.752 ± 0.016	6	7
		$1.6 \le \lvert y \rvert < 2.0$	2.298 ± 0.027	0.990 ± 0.020	1	3.700 ± 0.220	11.817 ± 0.528	0.432 ± 0.002	1	1.178 ± 0.012	2.686 ± 0.015	3	7
		$2.0 \le \lvert y \rvert < 2.4$	2.259 ± 0.022	0.953 ± 0.020	1	3.525 ± 0.200	11.482 ± 0.520	0.419 ± 0.002	1	1.122 ± 0.010	2.658 ± 0.015	1	7
Figure 4(c)		46-66	2.918 ± 0.011	0.987 ± 0.021	24	2.890 ± 0.175	8.152 ± 0.412	0.555 ± 0.002	18	1.164 ± 0.010	2.787 ± 0.016	50	7
		66-116	2.402 ± 0.022	1.038 ± 0.020	4	3.493 ± 0.209	10.540 ± 0.505	0.415 ± 0.002	4	1.290 ± 0.012	2.769 ± 0.015	12	12
		116-150	2.183 ± 0.011	1.008 ± 0.011	16	3.960 ± 0.221	12.841 ± 0.601	0.410 ± 0.002	10	1.371 ± 0.012	2.684 ± 0.014	40	7
Figure 4(d)	13000	66-116	2.177 ± 0.012	0.962 ± 0.018	11	3.862 ± 0.223	12.570 ± 0.603	0.428 ± 0.002	6	1.035 ± 0.010	2.550 ± 0.014	22	10
Figure 4(e)	7000	60-120	2.487 ± 0.020	1.071 ± 0.020	14	3.563 ± 0.205	10.390 ± 0.501	0.433 ± 0.002	5	1.373 ± 0.017	2.831 ± 0.011	24	6
	8000		2.341 ± 0.024	1.001 ± 0.019	7	3.441 ± 0.203	10.851 ± 0.505	0.409 ± 0.002	19	1.210 ± 0.015	2.719 ± 0.014	11	6
Figure 4(f)	7000	60-120	2.483 ± 0.011	0.936 ± 0.017	19	3.114 ± 0.183	9.211 ± 0.432	0.436 ± 0.002	32	1.214 ± 0.011	2.846 ± 0.015	36	8
	8000		3.438 ± 0.010	0.941 ± 0.017	15	3.121 ± 0.183	9.263 ± 0.431	0.433 ± 0.002	30	1.211 ± 0.011	2.810 ± 0.015	47	8
	13000		3.394 ± 0.045	0.996 ± 0.020	17	2.590 ± 0.129	4.653 ± 0.209	0.444 ± 0.002	36	1.170 ± 0.010	2.859 ± 0.015	16	8

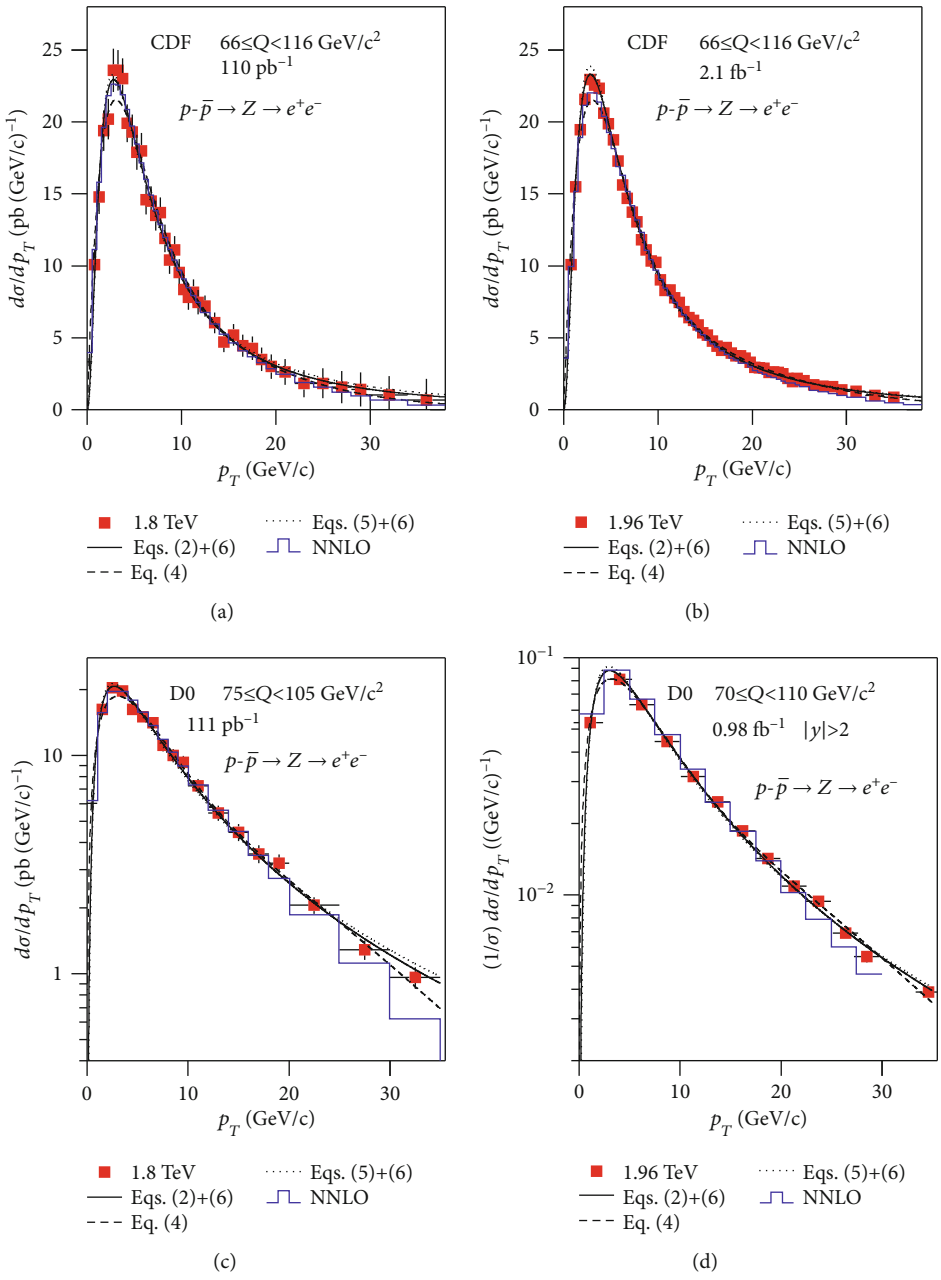

FIGURE 3: Same as Figure 2, but showing the p_T spectra of $\ell\bar{\ell}$ (with different invariant masses Q) produced by the Drell-Yan process in $p\bar{p}$ collisions at $\sqrt{s} = 1.8$ (a, c) and 1.96 TeV (b, d). The data points are quoted from the CDF (a, b) [48, 49] and D0 Collaborations (c, d) [50–52]. In all panels, $\ell\bar{\ell}$ is e^+e^-, see text in subsection 3.3 for the meanings of histograms which are quoted from QCD calculations.

and invariant mass. In Figures 7(a) and 7(b), one can see that the parameter p_1 has a slight tendency to increase with the increase of $\sqrt{s}$ and Q. In Figures 7(c) and 7(d), one can see that the parameter n_1 decreases quickly and then slowly with the increase of $\sqrt{s}$; n_1 also decreases slowly and then quickly with increase of Q. There is a boundary for the trend of n_1 at $\sqrt{s} \approx 40$–$200\,\text{GeV}$ and $Q \approx 20$–$50\,\text{GeV}/c^2$. We note that the variation of parameter is obtained from the the average values of the extracted parameters, for each $\sqrt{s}$ or Q.

It should be pointed out that the values of the parameters in Figures 5–7 are all obtained by fitting the experimental data in Figures 1–4 using the convolution of two Lévy-Tsallis functions, the two-component Erlang distribution, and the convolution of two Hagedorn functions, where the values obtained from Figures 1(e) and 1(f) are not included. Firstly, this is because the grouping of the quality in Figure 1(e) is different from the grouping of other data, and there are already many other groupings. Secondly, Figure 1(f) analyzes the p_T spectra within different ranges of Feynman variables, which is different from others in terms of event sample. To avoid trivialness, we have not put the fitting results of Figures 1(e) and 1(f) in Figures 5–7; though, these results are also shown in Table 1. We find that, by

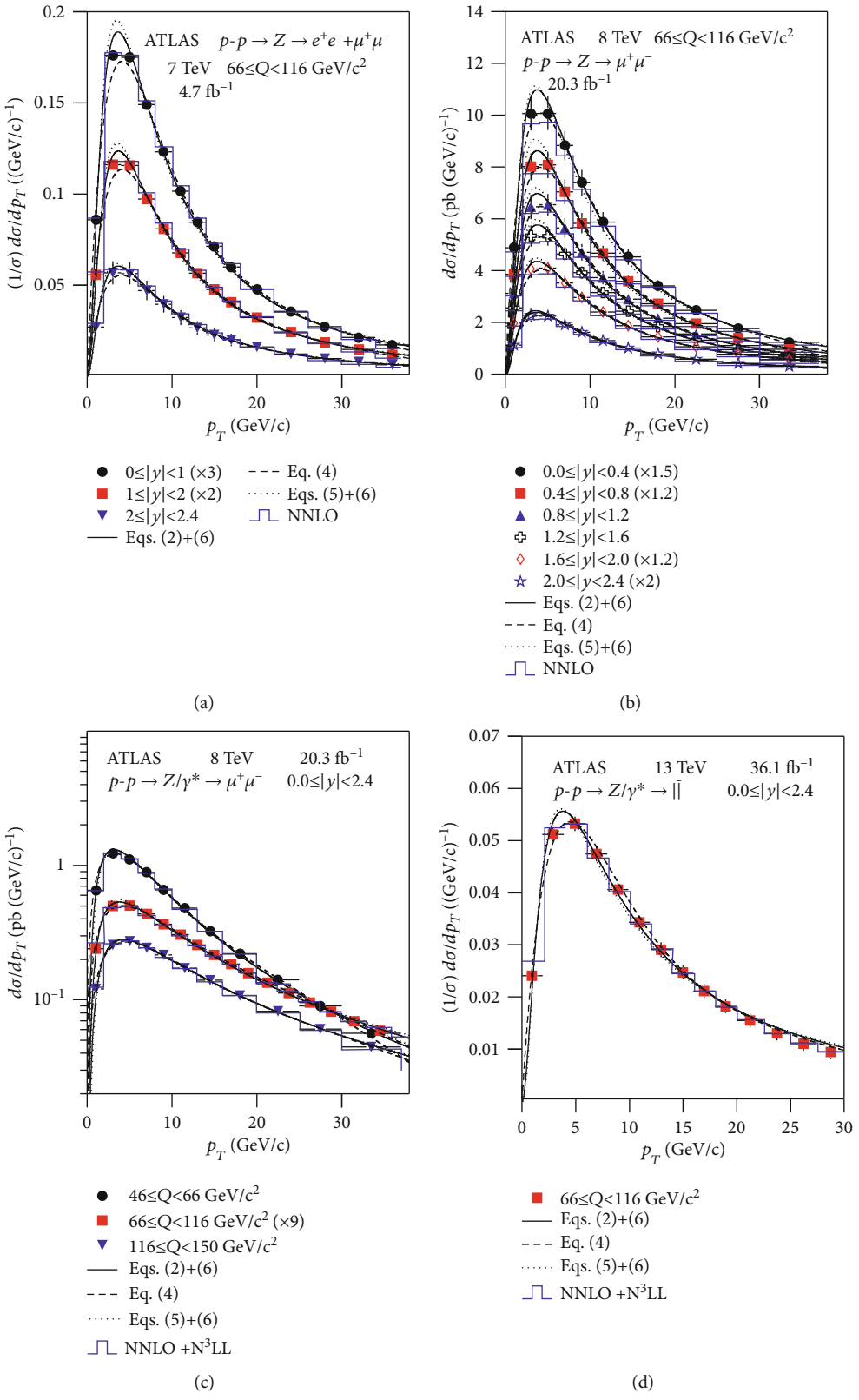

Figure 4: Continued.

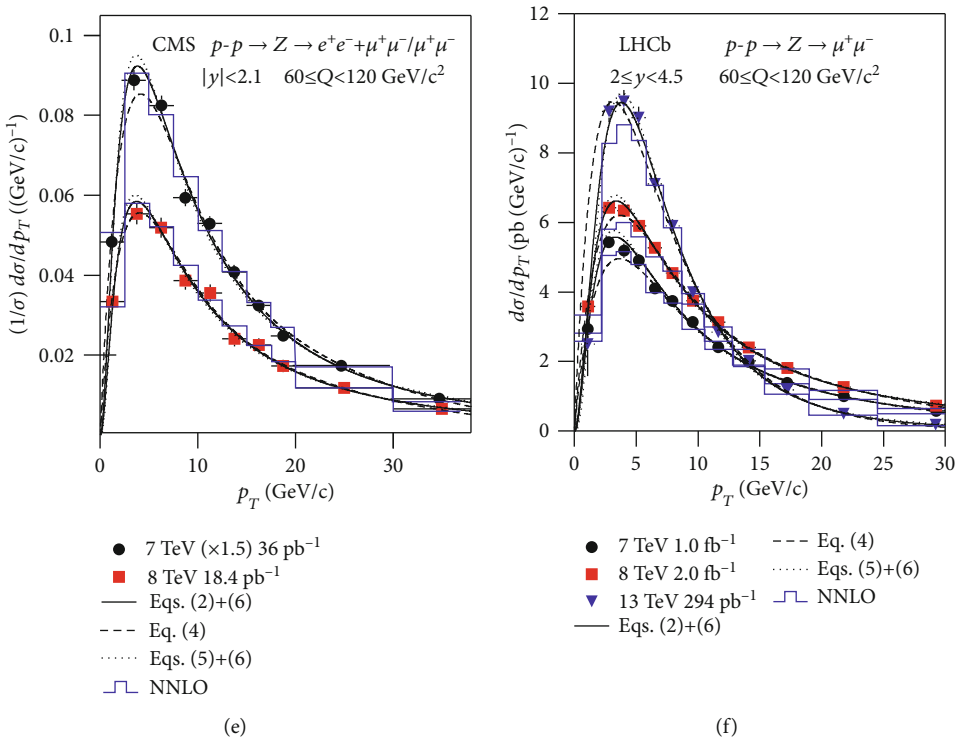

FIGURE 4: Same as Figure 2, but showing the p_T spectra of $\ell\bar{\ell}$ [with different conditions ($\sqrt{s}$, Q, and y)] produced by the Drell-Yan process in pp collisions at the LHC energies. The data points are quoted from the experiments performed by the ATLAS (a)–(d) [53–55], CMS (e) [56, 57], and LHCb Collaborations (f) [58–60]. The flavor of $\ell\bar{\ell}$ is shown in the panels, see text in subsection 3.3 for the meanings of histograms which are quoted from QCD calculations.

analyzing these results, they do not contradict the trend of other results presented in Figures 5–7.

The parameters T, $\langle p_t\rangle_S$, $\langle p_t\rangle_H$, and p_1 show monotonous increasing trend when $\sqrt{s}$ and Q increase. Naturally, the variation degrees are different. These increasing trends reflect that these parameters describe the violent degree of collisions between two (anti-)quarks in the Drell-Yan process. As the contribution fraction of the first component in the two-component Erlang distribution, k decreasing with increasing $\sqrt{s}$ and Q reflects naturally the increase of the contribution fraction of the second component. The parameter n increases firstly and then decreases, and the parameter n_1 decreases, with the increase of $\sqrt{s}$ and Q. This variation implies the change of interaction pattern and strength. A possible explanation is that the collision centrality between the two (anti-)quarks changes from periphery to center, or the violent degree of collisions increase, when $\sqrt{s}$ and Q increase. We should pay more attention on this variation in a future study.

In particular, the energy range considered in the present work is enough for the formation of QGP. It is possible that the p_T spectra of $\ell\bar{\ell}$ in the Drell-Yan process are affected by QGP. The nonmonotonous change of n implies the maximum influence between Drell-Yan and QGP. According to the Tsallis statistics, n is opposite to the entropy index q because $n = 1/(q-1)$. The maximum n at ~ 40 GeV implies that q is the closest to 1 at this energy. Meanwhile, at this energy, the system is the closest to the equilibrium. The softest point (~ 40 GeV) of equation of state from the excitation function of q is consistent with our very recent work [61] in which we stated that "the onset energy of the partial phase transition from hadron matter to QGP is 7.7 GeV and that of the whole phase transition is 39 GeV" with the uncertainty of 1–2 GeV.

We explain further the softest point here. In the energy range below ~ 40 GeV, there is not enough volume for the interactions between Drell-Yan and QGP due to partial phase transition [61]. In the energy range above ~ 40 GeV, there is not enough time for the interactions between Drell-Yan and QGP because the participants penetrate through each other quickly. Insufficient volume and time result in the system being not the closest to the equilibrium, though the system is still close to equilibrium at the softest point, $Q \approx 11$–18 GeV/c^2. At below (above) the softest point, we see naturally smaller (larger) Q, except for $Q = 5$–6 and 5–8 GeV/c^2 which show below the softest point at 20–30 GeV and also show above the softest point at 60–200 GeV, which should be studied in the future.

At the energy below 200 GeV and the invariant mass below 20 GeV/c^2, the system is close to the onset energy of phase transition. The parameters T, $\langle p_t\rangle_S$, $\langle p_t\rangle_H$, $1-k$, and p_1 show similar small and almost flat values, respectively, and n and n_1 show different trends. At the energy of TeV and the invariant mass around 100 GeV/c^2, the system is far away from the onset energy of phase transition. The parameters T, $\langle p_t\rangle_S$, $\langle p_t\rangle_H$, $1-k$, and p_1 show large values, and n

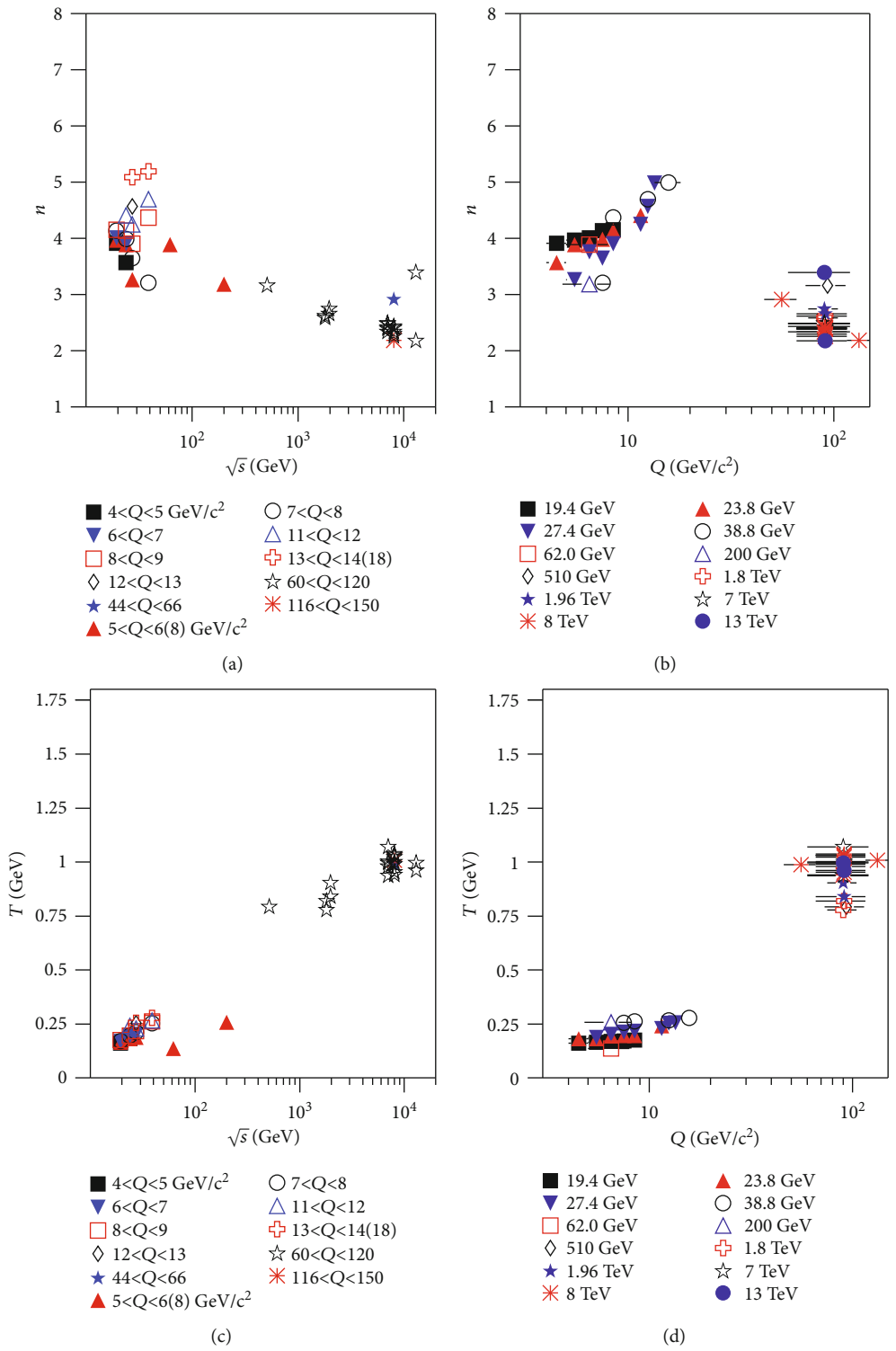

FIGURE 5: The variation of parameters n (a, b) and T (c, d) in the Lévy-Tsallis function with energy $\sqrt{s}$ (a, c) and invariant mass Q (b, d). The parameter values are taken from Figures 1–4 and recorded in Tables 1 and 2. Since the invariant mass grouping in Figure 1(e) is different from others, and the varying quantity in Figure 1(f) is the Feynman variable, Figure 5 does not include the parameters from Figures 1(e) and 1(f) to avoid trivialness.

and n_1 show a trend of decrease or saturation. These obvious characteristics in parameters make a clear distinction between approaching to and far away from the onset energy of phase transition from hadron matter to QGP because QGP also affects the spectra of $\ell\bar{\ell}$ in the Drell-Yan process.

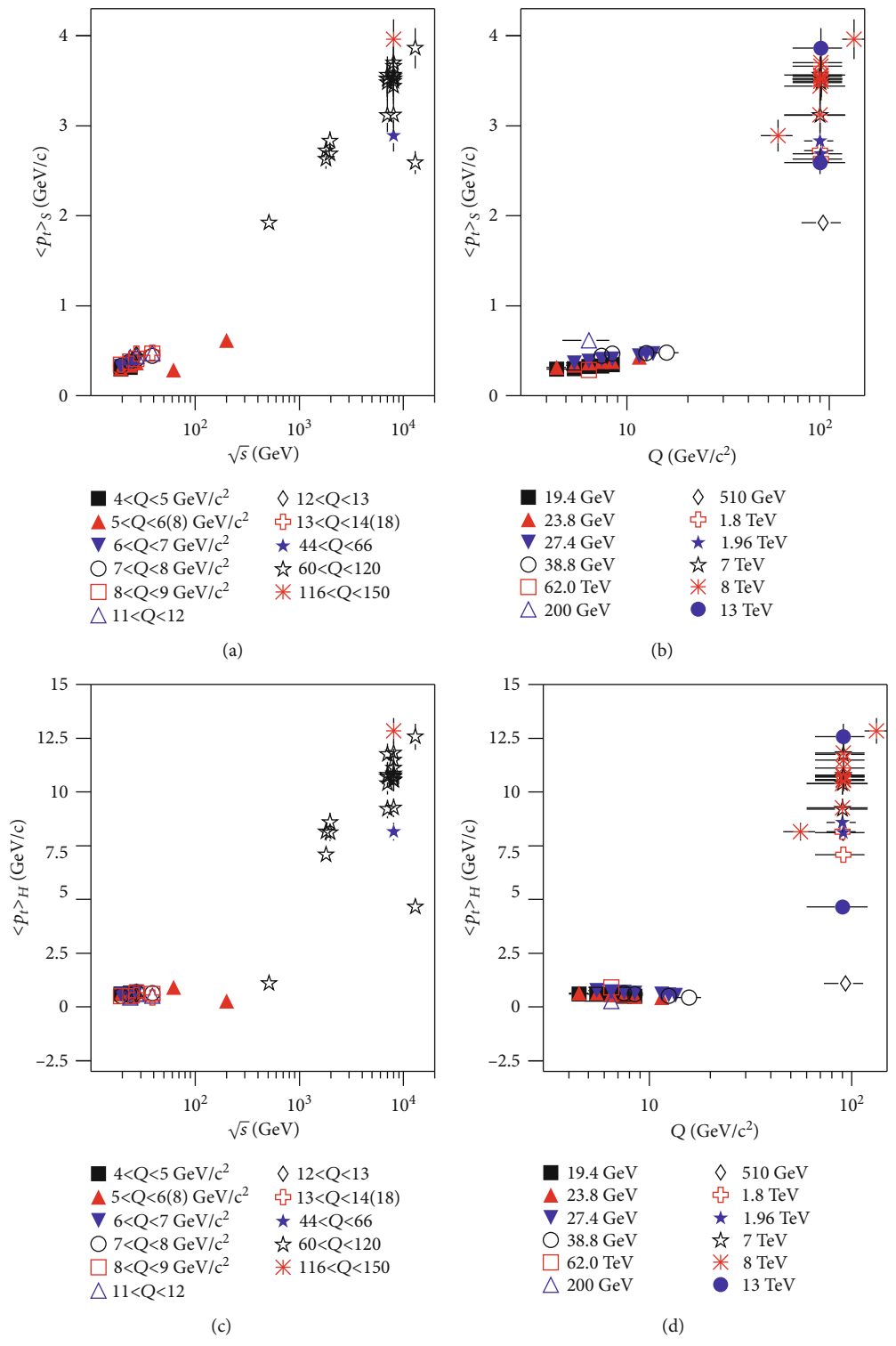

Figure 6: Continued.

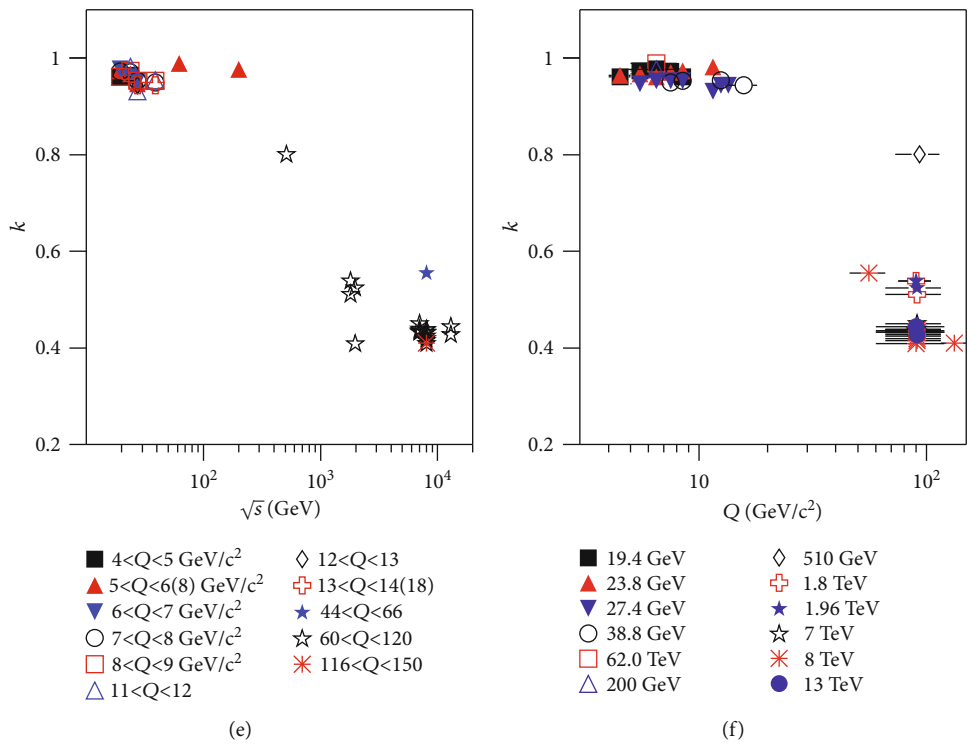

FIGURE 6: Similar to Figure 5, but showing the variation of parameters $\langle p_t \rangle_S$ (a, b), $\langle p_t \rangle_H$ (c, d), and k (e, f) in the two-component Erlang distribution with $\sqrt{s}$ (a, c, e) and Q (b, d, f).

3.3. Further Discussion. In the exact factorization formula, the true TMD parton distributions depend on the hard scale of the process (for the Drell-Yan process, the invariant mass Q of $\ell\bar{\ell}$) and obey renormalization group equations. Although this scaling is not included in the function $f_1(p_{t1})$ or $f_1(p_T - p_{t1})$ of Eq. (6), it reappears through the dependence of its parameters upon Q (and also the center-of-mass energy squared s). The dependence of the parameters on Q reflects the fact that the function $f_1(p_{t1})$ or $f_1(p_T - p_{t1})$ must change its parameters with the hard scale. This result is consistent with the appropriate frameworks: collinear framework for large transverse momentum and TMD framework for small transverse momentum [2].

In addition, the formulae for the evolution of TMD parton distributions are rather complicated, and the resulting effect is difficult to parameterize with simple expressions. The present work is a preliminary attempt for the purpose of parameterization with simple expressions. Meanwhile, as a preliminary attempt, the present work is not accurate in some cases which show large χ^2/ndof. In other cases, χ^2/ndof is approximately 1 or not too large. In any case, we firmly believe that the underlying physics law is knowable and simple. A very complicated expression for the transverse momentum spectra of $\ell\bar{\ell}$ in the Drell-Yan process in high-energy collisions is not the final one. More work for simplifying the expressions is needed in the future.

After describing the spectra of $\ell\bar{\ell}$ in the Drell-Yan process, it is possible to subtract the contribution of the Drell-Yan process from the spectra of $\ell\bar{\ell}$ in the final state and leave behind only the contribution of QGP. Then, one may study the excitation function of related parameters from the spectra of $\ell\bar{\ell}$ contributed purely in QGP conditions and search for the softest points of equation of state from the excitation function. The energies corresponding to the softest points are expected to connect with the critical energy of phase transition from hadron matter to QGP. If both the spectra of $\ell\bar{\ell}$ in the Drell-Yan process and in QGP degeneration process are described by simple functions, one can study the phase transition more conveniently. We hope that the present work is significant in methodology for the study in the future.

We now discuss the results as they pertain to QCD calculations [23, 24, 46, 55, 62–64]. To study more deeply, and in a visual way, the connection between our formalism and the standard QCD resummation, we present a direct comparison in Figures 1–4 as examples. As can be seen, the histograms presented in Figures 1–4 represent the results with different treatments based on QCD calculations, which will be discussed separately in the following.

The histograms in Figures 1(a)–1(d) are directly quoted from those in ref. [23] in which the next-to-next-to-leading order (NNLO) calculation is performed for nonperturbative structure of semi-inclusive deep-inelastic scattering and the Drell-Yan scattering at small transverse momentum within TMD factorization. The histograms in Figures 1(e) and 1(f) are directly quoted from those in ref. [62] in which the NNLO calculation is performed for the Drell-Yan processes within TMD factorization. In the figure, some histograms are renormalized to the data to give a better comparison.

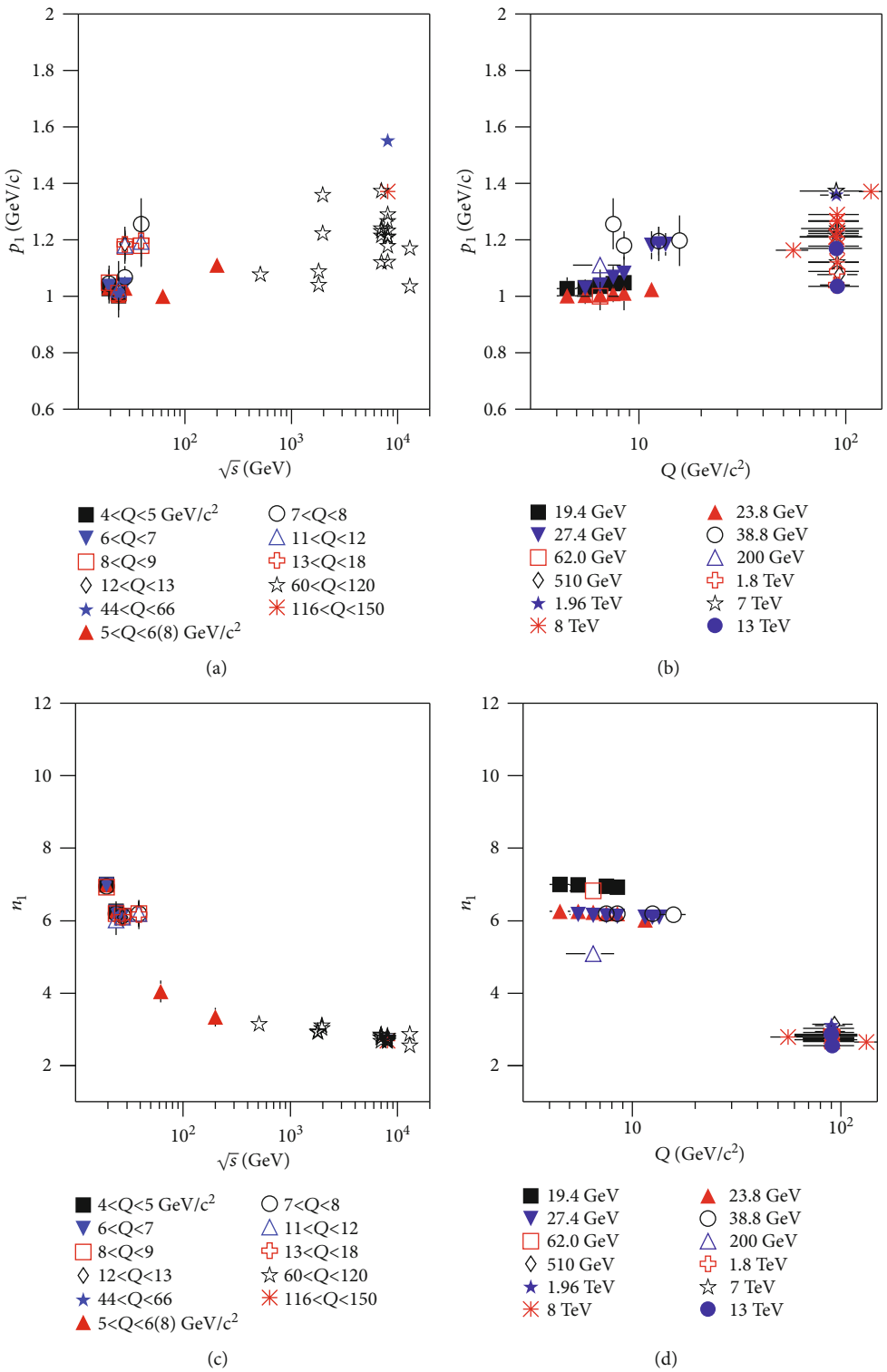

FIGURE 7: Similar to Figure 5, but showing the parameters p_1 (a, b) and n_1 (c, d) in the Hagedorn function with (a) (c) $\sqrt{s}$ and (b) (d) Q.

The histogram in Figure 2(a) is transformed from the curve in ref. [46] to fit the style of other panels and to give a clear display. In the transformation from the curve to histogram, the areas under the histogram and curve in a given transverse momentum bin are kept being the same. In ref. [46], the calculation of QCD convoluted with the Gaussian function is used. The histogram in Figure 2(b) is directly quoted from that in ref. [63] in which the transverse momentum spectrum of low invariant mass Drell-Yan is produced at next-to-leading order (NLO) in the parton branching method. The histogram in Figure 2(c) is directly quoted from that in ref. [24] in which the TMD parton distributions are

considered up to next-to-next-to-next-to-leading order logarithmic (N^3LO or N^3LL) from the Drell-Yan data.

The meanings of histograms in Figure 3 and Figure 4(a), Figure 4(b), Figure 4(c) with $46 \le Q < 66$ and $116 \le Q < 150$ GeV/c^2, Figure 4(e), and Figure 4(f) are the same as Figures 1(a)–1(d), which will not be discussed anymore. The histogram in Figure 4(c) with $66 \le Q < 116$ GeV/c^2 is directly quoted from that in ref. [64] in which the calculation is performed due to the Drell-Yan transverse momentum resummation of fiducial power corrections at N^3LL. The histograms in Figure 4(d) are directly quoted from those in ref. [55] in which the transverse momentum distributions of the Drell-Yan $\ell\bar{\ell}$ are calculated up to NNLO + N^3LL.

From the above descriptions, one can see that the formalism of this paper is flexible in the fit to data. We may compare the fits with more QCD predictions, and it does not matter with or without the TMD PDFs. Except for several papers in which the Drell-Yan transverse momentum spectrum is predicted based on QCD factorization are referenced in the introduction [23, 24] and the above discussion [46, 55, 62–64], more works related to the PDFs or TMDs in QCD are available recently [65–74]. These QCD factorizations are complex in the calculation and show different forms of formalization from this paper but result in similar shapes for the dilepton spectra as observed in experiments. By adjusting the parameters, the formalism of this paper can flexibly fit the QCD predictions with or without the TMD PDFs. Compared to predictions from collinear PDFs, the formalism of this paper is closer to TMD PDFs due to the flexible parameter selection in the fit. The PDFs or TMDs in QCD and other QCD-based analyses reveal the dynamic aspect of the particle production process. The formalism used by us reflects the statistical behavior of the produced particles.

4. Summary and Conclusions

We have studied the transverse momentum spectra of lepton pairs generated by the Drell-Yan process in p-Cu, π^--W, and pp ($p\bar{p}$) collisions over an energy range from ~ 20 GeV to above 10 TeV. The low-energy data come from the E288, E605, R209, PHENIX, and STAR Collaborations. The high-energy data come from the CDF, D0, ATLAS, CMS, and LHCb Collaborations. The invariant mass range of the final-state particles produced in the collisions also has a large span of $4 < Q < 150$GeV/c^2. Three types of probability density functions are used to fit and analyze the collected experimental data. All the three functions are approximately in agreement with the experimental data and the QCD calculations. Some parameters are obtained.

In the convolution of two Lévy-Tsallis functions, as increasing $\sqrt{s}$, there is a knee point for the trend of n at $\sqrt{s} \approx 40$–50 GeV. Meanwhile, there is a boundary at $\sqrt{s} \approx 200$–500 GeV above which T increases significantly. With the increase of Q, there is a knee point for the trend of n at $Q \approx 14$–15 GeV/c^2. Meanwhile, there is a boundary at $Q \approx 20$–60 GeV/c^2 above which T increases significantly. In the two-component Erlang distribution, there is a boundary at $\sqrt{s} \approx 60$–500 GeV for $\langle p_t \rangle_S$, 500–1100 GeV for $\langle p_t \rangle_H$, and 200–500 GeV for k, above which $\langle p_t \rangle_S$, $\langle p_t \rangle_H$, and $1 - k$ increase quickly. Meanwhile, there is a boundary at $Q \approx 20$–60 GeV/c^2 above which $\langle p_t \rangle_S$, $\langle p_t \rangle_H$, and $1 - k$ increase quickly. In the convolution of two Hagedorn functions, p_1 increases obviously with increasing $\sqrt{s}$ and Q. There is a boundary for the trend of n_1 at $\sqrt{s} \approx 40$–200 GeV and $Q \approx 20$–50 GeV/c^2.

With increasing $\sqrt{s}$ and Q, the parameters T, $\langle p_t \rangle_S$, $\langle p_t \rangle_H$, $1 - k$, and p_1 show monotonous increasing trend. These increasing trends reflect that these parameters describe the violent degree of collisions between quark and antiquark in the Drell-Yan process. The parameter n increases initially and then decreases, and the parameter n_1 decreases, with the increase of $\sqrt{s}$ and Q. This variation implies the change of interaction pattern and strength. A possible explanation is that the collision centrality between quark and antiquark changes from periphery to center, or the violent degree of collisions increases, when $\sqrt{s}$ and Q increase. The fit results in this paper are comparable to the QCD NNLO and N^3LL results with TMD PDFs.

In conclusion, the large number of events collected by the investigated experiments allows us to study the statistical behavior of dilepton production in hadron and nuclei collisions. The lepton pairs can be produced through the Drell-Yan process and the QGP degeneration process. Both processes are predicted by QCD and are described well enough by our statistical thermodynamics models, especially in kinematic regions with sufficiently large numbers of events.

Data Availability

The data used to support the findings of this study are included within the article and are cited at relevant places within the text as references.

Ethical Approval

The authors declare that they are in compliance with ethical standards regarding the content of this paper.

Disclosure

The funding agencies have no role in the design of the study; in the collection, analysis, or interpretation of the data; in the writing of the manuscript; or in the decision to publish the results.

Conflicts of Interest

The authors declare that there are no conflicts of interest regarding the publication of this paper.

Acknowledgments

X.-H. Zhang and F.-H. Liu's work was supported by the National Natural Science Foundation of China under Grant Nos. 12047571, 11575103, and 11947418, the Scientific and Technological Innovation Programs of Higher Education Institutions in Shanxi (STIP) under Grant No. 201802017,

the Shanxi Provincial Natural Science Foundation under Grant No. 201901D111043, and the Fund for Shanxi "1331 Project" Key Subjects Construction.

References

[1] S. Drell and T.-M. Yan, "Massive lepton pair production in hadron-hadron collisions at high-energies," *Physical Review Letters*, vol. 25, pp. 316–320, 1970.

[2] J. Collins, *Foundations of Perturbative QCD*, Cambridge University Press, London, UK, 2011.

[3] J. C. Collins, D. E. Soper, and G. Sterman, "Transverse momentum distribution in Drell-Yan pair and W and Z boson production," *Nuclear Physics B*, vol. 250, pp. 199–224, 1985.

[4] T. C. Rogers, "An overview of transverse-momentum-dependent factorization and evolution," *The European Physical Journal A*, vol. 52, p. 153, 2016.

[5] M. Diehl, "Introduction to GPDs and TMDs," *The European Physical Journal A*, vol. 52, p. 149, 2016.

[6] R. Angeles-Martinez, A. Bacchetta, I. I. Balitsky et al., "Transverse momentum dependent (TMD) parton distribution functions: status and prospects," *Acta Physica Polonica B*, vol. 46, pp. 2501–2534, 2015.

[7] G. Bozzi, S. Catani, G. Ferrera, D. de Florian, and M. Grazzini, "Production of Drell-Yan lepton pairs in hadron collisions: transverse-momentum resummation at next-to-next-to-leading logarithmic accuracy," *Physics Letters B*, vol. 696, no. 3, pp. 207–213, 2011.

[8] S. Catani, L. Cieri, D. de Florian, G. Ferrera, and M. Grazzini, "Vector boson production at hadron colliders: hard-collinear coefficients at the NNLO," *The European Physical Journal C*, vol. 72, p. 2195, 2012.

[9] J. Collins, L. Gamberg, A. Prokudin, T. C. Rogers, N. Sato, and B. Wang, "Relating transverse momentum dependent and collinear factorization theorems in a generalized formalism," *Physical Review D*, vol. 94, article 034014, 2016.

[10] C. T. H. Davies, B. R. Webber, and W. Stirling, "Drell-Yan cross-sections at small transverse momentum," *Nuclear Physics B*, vol. 256, pp. 413–433, 1985.

[11] G. A. Ladinsky and C.-P. Yuan, "The nonperturbative regime in QCD resummation for gauge boson production at hadron colliders," *Physical Review D*, vol. 50, pp. 4239(R)–4243(R), 1994.

[12] F. Landry, R. Brock, G. Ladinsky, and C.-P. Yuan, "New fits for the non-perturbative parameters in the CSS resummation formalism," *Physical Review D*, vol. 63, article 013004, 2001.

[13] J.-W. Qiu and X.-F. Zhang, "Role of the nonperturbative input in QCD resummed Drell-Yan QT distributions," *Physical Review D*, vol. 67, article 114011, 2001.

[14] F. Landry, R. Brock, P. M. Nadolsky, and C.-P. Yuan, "Tevatron Run-1 Z boson data and Collins-Soper-Sterman resummation formalism," *Physical Review D*, vol. 67, article 073016, 2003.

[15] A. V. Konychev and P. M. Nadolsky, "Universality of the Collins-Soper-Sterman nonperturbative function in gauge boson production," *Physics Letters B*, vol. 633, pp. 710–714, 2006.

[16] T. Becher, M. Neubert, and D. Wilhelm, "Electroweak gauge-boson production at small q_T: Infrared safety from collinear anomaly," *Journal of High Energy Physics*, vol. 2012, no. 2, article 124, 2012.

[17] U. D'Alesio, M. G. Echevarria, S. Melis, and I. Scimemi, "Nonperturbative QCD effects in qT spectra of Drell-Yan and Z-boson production," *Journal of High Energy Physics*, vol. 2014, no. 11, article 98, 2014.

[18] M. G. Echevarria, A. Idilbi, Z.-B. Kang, and I. Vitev, "QCD evolution of the Sivers asymmetry," *Physical Review D*, vol. 89, article 074013, 2014.

[19] A. Bacchetta, F. Delcarro, C. Pisano, M. Radici, and A. Signori, "Extraction of partonic transverse momentum distributions from semi-inclusive deep-inelastic scattering, Drell-Yan and Z-boson production," *Journal of High Energy Physics*, vol. 2017, no. 6, article 81, 2017.

[20] I. Scimemi and A. Vladimirov, "Analysis of vector boson production within TMD factorization," *The European Physical Journal C*, vol. 78, p. 89, 2018.

[21] P. Sun, J. Isaacson, C.-P. Yuan, and F. Yuan, "Nonperturbative functions for SIDIS and Drell-Yan processes," *International Journal of Modern Physics A*, vol. 33, article 1841006, 2018.

[22] V. Bertone, I. Scimemi, and A. Vladimirov, "Extraction of unpolarized quark transverse momentum dependent parton distributions from Drell-Yan/Z-boson production," *Journal of High Energy Physics*, vol. 2019, no. 6, p. 28, 2019.

[23] I. Scimemi and A. Vladimirov, "Nonperturbative structure of semi-inclusive deep-inelastic and Drell-Yan scattering at small transverse momentum," *Journal of High Energy Physics*, vol. 2020, no. 6, article 137, 2020.

[24] A. Bacchetta, V. Bertone, C. Bissolotti et al., "Transverse-momentum-dependent parton distributions up to N^3LL from Drell-Yan data," *Journal of High Energy Physics*, vol. 2020, no. 7, article 117, 2020.

[25] S. Camarda, M. Boonekamp, G. Bozzi et al., "DYTurbo: fast predictions for Drell-Yan processes," *The European Physical Journal C*, vol. 80, p. 251, 2020.

[26] C. Tsallis, "Possible generalization of Boltzmann-Gibbs statistics," *Journal of Statistical Physics*, vol. 52, pp. 479–487, 1988.

[27] J. Adams and et al.STAR Collaboration, "K(892)$*$ resonance production in Au+Au and p+p collisions at $\sqrt{s_{NN}} = 200$ GeV," *Physical Review C*, vol. 75, article 064901, 2007.

[28] S. Song, X. R. Gou, F. L. Shao, and Z. T. Liang, "Quark number scaling of hadronic p_T spectra and constituent quark degree of freedom in p-Pb collisions at $\sqrt{s_{NN}} = 5.02$ TeV," *Physics Letters B*, vol. 774, pp. 516–521, 2017.

[29] Z. B. Tang, Y. C. Xu, L. J. Ruan, G. van Buren, F. Q. Wang, and Z. B. Xu, "Spectra and radial flow in relativistic heavy ion collisions with Tsallis statistics in a blast-wave description," *Physical Review C*, vol. 79, article 051901(R), 2009.

[30] P. N. Rathie and S. Da Silva, "Shannon, Lévy, and Tsallis: a note," *Applied Mathematical Sciences (HIKARI)*, vol. 2, no. 28, pp. 1359–1363, 2008.

[31] F.-H. Liu and J.-S. Li, "Isotopic production cross section of fragments in ^{56}Fe+p and ^{136}Xe(^{124}Xe)+Pb reactions over an energy range from 300A to 1500A MeV," *Physical Review C*, vol. 78, article 044602, 2008.

[32] F.-H. Liu, "Unified description of multiplicity distributions of final-state particles produced in collisions at high energies," *Nuclear Physics A*, vol. 810, pp. 159–172, 2008.

[33] F.-H. Liu, Y.-Q. Gao, T. Tian, and B.-C. Li, "Unified description of transverse momentum spectrums contributed by soft and hard processes in high energy nuclear collisions," *The European Physical Journal A*, vol. 50, article 94, 2014.

[34] H. Hagedorn, "Multiplicities, p_T distributions and the expected hadron⟶quark-gluon phase transition," *La Rivista del Nuovo Cimento*, vol. 6, no. 10, pp. 1–50, 1983.

[35] B. Abelev and et al.ALICE Collaboration, "Production of $\sum(1385)^{\pm}$ and $\sum(1530)^{0}$ in proton-proton collisions at $\sqrt{s} = 7$ TeV," *The European Physical Journal C*, vol. 75, p. 1, 2015.

[36] E. Schnedermann, J. Sollfrank, and U. Heinz, "Thermal phenomenology of hadrons from 200A GeV S+S collisions," *Physical Review C*, vol. 48, pp. 2462–2475, 1993.

[37] B. I. Abelev, M. M. Aggarwal, Z. Ahammed et al., "Systematic measurements of identified particle spectra in pp, d+Au, and Au+Au collisions at the STAR detector," *Physical Review C*, vol. 79, article 034909, 2009.

[38] B. I. Abelev, M. M. Aggarwal, Z. Ahammed et al., "Identified particle production, azimuthal anisotropy, and interferometry measurements in Au+Au collisions at $\sqrt{s_{NN}} = 9.2$ GeV," *Physical Review C*, vol. 81, article 024911, 2010.

[39] Z.-J. Xiao and C.-D. Lü, *Introduction to Particle Physics*, Science Press, Beijing, China, 2016.

[40] F.-H. Liu, "Particle production in Au-Au collisions at RHIC energies," *Physical Letters B*, vol. 583, pp. 68–72, 2004.

[41] P.-P. Yang, F.-H. Liu, and R. Sahoo, "A new description of transverse momentum spectra of identified particles produced in proton-proton collisions at high energies," *Advances in High Energy Physics*, vol. 2020, Article ID 6742578, 16 pages, 2020.

[42] P.-P. Yang, M.-Y. Duan, and F.-H. Liu, "Dependence of related parameters on centrality and mass in a new treatment for transverse momentum spectra in high energy collisions," *The European Physical Journal A*, vol. 57, p. 63, 2021.

[43] A. S. Ito, R. J. Fisk, and H. Jöstlein, "Measurement of the continuum of dimuons produced in high energy proton-nucleus collisions," *Physical Review D*, vol. 23, pp. 604–633, 1981.

[44] G. Moreno, C. N. Brown, W. E. Cooper et al., "Dimuon production in proton-copper collisions at $\sqrt{s} = 38.8$GeV," *Physical Review D*, vol. 43, pp. 2815–2836, 1991.

[45] W. J. Stirling and M. R. Whalley, "A compilation of Drell-Yan cross sections," *Journal of Physics G*, vol. 19, pp. D1–D102, 1993.

[46] D. Antreasyan, U. Becker, G. Bellettini et al., "Dimuon scaling comparison at 44 and 62 GeV," *Physical Review Letters*, vol. 48, pp. 302–304, 1982.

[47] C. Aidala, Y. Akiba, M. Alfred et al., "Measurements of $\mu\mu$ pairs from open heavy flavor and Drell-Yan in p+p collisions at $\sqrt{s} = 200$GeV," *Physical Review D*, vol. 99, article 0720033, 2019.

[48] T. Affolder and et al.CDF collaboration, "The transverse momentum and total cross section of e^+e^- pairs in the Z boson region from $p\bar{p}$ collisions at $\sqrt{s} = 1.8$TeV," *Physical Review Letters*, vol. 84, pp. 845–850, 2000.

[49] T. Aaltonen, B. A. González, S. Amerio et al., "Transverse momentum cross section of e^+e^- pairs in the Z-boson region from $p\bar{p}$ collisions at $\sqrt{s} = 1.96$TeV," *Physical Review D*, vol. 86, article 052010, 2012.

[50] B. Abbott, M. Abolins, V. Abramov et al., "Measurement of the inclusive differential cross section for Z bosons as a function of transverse momentum in $p\bar{p}$ collisions at $\sqrt{s} = 1.8$TeV," *Physical Review D*, vol. 61, article 032004, 2000.

[51] V. M. Abazov, B. Abbott, M. Abolins et al., "Measurement of the shape of the boson transverse momentum distribution in $p\bar{p} \longrightarrow Z/\gamma^* \longrightarrow e^+e^- + X$ events produced at $\sqrt{s} = 1.96$TeV," *Physical Review Letters*, vol. 100, article 102002, 2008.

[52] V. M. Abazov, B. Abbott, M. Abolins et al., "Measurement of the normalized $Z/\gamma^* \longrightarrow \mu^+\mu^-$ transverse momentum distribution in $p\bar{p}$ collisions at $\sqrt{s} = 1.96$TeV," *Physics Letters B*, vol. 693, pp. 522–530, 2010.

[53] G. Aad, B. Abbott, J. Abdallah et al., "Measurement of the Z/γ^* boson transverse momentum distribution in pp collisions at $\sqrt{s} = 7$TeV with the ATLAS detector," *Journal of High Energy Physics*, vol. 2014, no. 9, article 145, 2014.

[54] G. Aad, B. Abbott, J. Abdallah et al., "Measurement of the transverse momentum and ϕ_η^* distributions of Drell-Yan lepton pairs in proton-proton collisions at $\sqrt{s} = 8$TeV with the ATLAS detector," *The European Physical Journal C*, vol. 76, article 291, 2016.

[55] M. Aaboud, G. Aad, B. Abbott et al., "Measurement of the transverse momentum distribution of Drell-Yan lepton pairs in proton-proton collisions at $\sqrt{s} = 13$TeV with the ATLAS detector," *The European Physical Journal C*, vol. 80, article 616, 2020.

[56] S. Chatrchyan, V. Khachatryan, A. M. Sirunyan et al., "Measurement of the rapidity and transverse momentum distributions of Z bosons in pp collisions at $\sqrt{s} = 7$TeV," *Physical Review D*, vol. 85, article 032002, 2012.

[57] V. Khachatryan, A. M. Sirunyan, A. Tumasyan et al., "Measurement of the transverse momentum spectra of weak vector bosons produced in proton-proton collisions at $\sqrt{s} = 8$TeV," *Journal of High Energy Physics*, vol. 2017, no. 2, p. 96, 2017.

[58] A. Aaij and et al.LHCb collaboration, "Measurement of the forward Z boson production cross-section in pp collisions at $\sqrt{s} = 7$TeV," *Journal of High Energy Physics*, vol. 2015, no. 8, p. 39, 2015.

[59] R. Aaij, C. A. Beteta, B. Adeva et al., "Measurement of forward W and Z boson production in pp collisions at $\sqrt{s} = 8$TeV," *Journal of High Energy Physics*, vol. 2016, no. 1, p. 155, 2016.

[60] A. Aaij and et al.LHCb collaboration, "Measurement of the forward Z boson production cross-section in pp collisions at $\sqrt{s} = 13$TeV," *Journal of High Energy Physics*, vol. 2016, no. 9, p. 136, 2016.

[61] M. Waqas, F.-H. Liu, R.-Q. Wang, and I. Siddique, "Energy scan/dependence of kinetic freeze-out scenarios of multistrange and other identified particles in central nucleus–nucleus collisions," *The European Physical Journal A*, vol. 56, article 188, 2020.

[62] A. Vladimirov, "Pion-induced Drell-Yan processes within TMD factorization," *Journal of High Energy Physics*, vol. 2019, no. 10, article 90, 2019.

[63] A. B. Martinez, P. L. S. Connor, D. D. Damiani et al., "The transverse momentum spectrum of low mass Drell-Yan production at next-to-leading order in the parton branching method," *The European Physical Journal C*, vol. 80, p. 598, 2020.

[64] M. A. Ebert, J. K. L. Michel, L. W. Stewart, and F. J. Tackmann, "Drell-Yan q_T resummation of fiducial power corrections at N^3LL," *Journal of High Energy Physics*, vol. 2021, no. 4, artile 102, 2021.

[65] V. E. Lyubovitskij and I. Schmidt, "Scaling of PDFs, TMDs, and GPDs in soft-wall AdS/QCD," *Physical Review D*, vol. 102, article 034011, 2020.

[66] C. Shugert, X. Gao, T. Izubuchi et al., "Pion valence quark PDF from lattice QCD," in *Proceedings of the 37th International Symposium on Lattice Field Theory – Lattice 2019*, Wuhan, China, 2019.

[67] E. R. Nocera, M. Ubiali, and C. Voisey, "Single top production in PDF fits," *Journal of High Energy Physics*, vol. 20, no. 5, artile 67, 2020.

[68] A. Lelek, "The role of angular ordering condition in parton branching transverse momentum dependent (TMD) PDFs and DY transverse momentum spectrum at LHC," in *Proceedings of the European Physical Society Conference on High Energy Physics–EPS-HEP2019*, Ghent, Belgium, 2019.

[69] S. Bailey and L. A. Harland-Lang, "Differential top quark pair production at the LHC: challenges for PDF fits," *The European Physical Journal C*, vol. 80, aticle 60, 2020.

[70] C. A. Flett, S. P. Jones, A. D. Martin, M. G. Ryskin, and T. Teubner, "How to include exclusive J/ψ production data in global PDF analyses," *Physical Review D*, vol. 101, article 094011, 2020.

[71] M. A. Ebert, B. Mistlberger, and G. Vita, "Transverse momentum dependent PDFs at N^3LO," *Journal of High Energy Physics*, vol. 2020, no. 9, article 46, 2020.

[72] S. Alekhin, J. Blümlein, and S. Moch, "Heavy-flavor PDF evolution and variable-flavor number scheme uncertainties in deep-inelastic scattering," *Physical Review D*, vol. 102, article 054014, 2020.

[73] Z.-Y. Li, Y.-Q. Ma, and J.-W. Qiu, "Extraction of Next-to-Next-to-Leading-Order PDFs from Lattice QCD Calculations," *Physical Review Letters*, vol. 126, article 072001, 2008.

[74] M. A. Nefedov and V. A. Saleev, "High-energy factorization for Drell-Yan process in pp and $p\bar{p}$ collisions with new unintegrated PDFs," *Physical Review D*, vol. 102, article 114018, 2020.